

Effect of symmetric and asymmetric substitution on the optoelectronic properties of 9,10-dicyanoanthracene

Supporting Information

F. Glöcklhofer¹, A. Rosspeintner², P. Pasitsuparoad³, S. Eder², J. Fröhlich²,
G. Angulo³, E. Vauthey¹, and F. Plasser⁴

¹Institute of Applied Synthetic Chemistry, TU Wien, AT-1060 Vienna, Austria

²Department of Physical Chemistry, University of Geneva, CH-1211 Geneva, Switzerland

³Institute of Physical Chemistry, Polish Academy of Sciences, 01-224 Warsaw, Poland

⁴Department of Chemistry, Loughborough University, LE11 3TU, United Kingdom

Contents

| | | |
|----------|---|------------|
| 1 | Materials | S3 |
| 1.1 | Photophysics and Electrochemistry | S3 |
| 1.2 | Synthesis | S3 |
| 2 | Experimental Methods | S3 |
| 2.1 | NMR Spectroscopy | S3 |
| 2.2 | Electrochemistry | S3 |
| 2.3 | One-Photon (1P) Spectroscopy | S3 |
| 2.4 | Time-Resolved Fluorescence | S4 |
| 2.5 | Two-Photon (2P) Spectroscopy | S5 |
| 2.6 | Quantum Chemical Calculations | S5 |
| 2.6.1 | Computational Details | S5 |
| 2.6.2 | Integrated 1P absorption cross section | S5 |
| 2.6.3 | Integrated 2P absorption cross section | S6 |
| 3 | Synthesis | S7 |
| 3.1 | Methoxy-substituted anthraquinones 2a-b | S7 |
| 3.2 | General procedure for the synthesis of methoxy-substituted DCAs D1 and Q1 . . | S7 |
| 3.3 | Synthesis of anthraquinone triflates 3a-b | S8 |
| 3.4 | Synthesis of DCA triflates 4a-b | S8 |
| 3.5 | Synthesis of 4-methoxyphenyl-substituted DCAs D2 and Q2 | S8 |
| 3.6 | Synthesis of (4-methoxyphenyl)ethynyl-substituted DCAs D3 and Q3 | S9 |
| 4 | Additional Experimental Results | S10 |
| 4.1 | Electrochemistry | S10 |
| 4.2 | Photophysics | S12 |
| 4.2.1 | Solvatochromism | S12 |
| 4.2.2 | Mirror Symmetry Relation | S14 |

| | | |
|---|--|-----|
| 5 | Effect of molecular size on fluorescence solvatochromism | S16 |
| 6 | Time-resolved Emission Data | S17 |
| 7 | Additional Computational Results | S19 |
| 8 | NMR Spectra | S27 |

List of Figures

| | | |
|----|---|-----|
| 1 | Cyclic voltammograms | S11 |
| 2 | Solvent dependence of absorption and fluorescence of DCA . | S12 |
| 3 | Solvent dependence of absorption and emission spectra | S13 |
| 4 | Residuals of the solvatochromic plots | S14 |
| 5 | Mirror symmetry of A and DCA | S14 |
| 6 | Mirror symmetry of Ds and Qs | S15 |
| 7 | Calculated permanent and transition dipole (quadrupole) moments D1 | S21 |
| 8 | Calculated permanent and transition dipole (quadrupole) moments D2 | S22 |
| 9 | Calculated permanent and transition dipole (quadrupole) moments D3 | S23 |
| 10 | Calculated permanent and transition dipole (quadrupole) moments Q1 | S24 |
| 11 | Calculated permanent and transition dipole (quadrupole) moments Q2 | S25 |
| 12 | Calculated permanent and transition dipole (quadrupole) moments Q3 | S26 |
| 13 | ¹ H and ¹³ C-NMR spectra of 2a . | S27 |
| 14 | ¹ H and ¹³ C-NMR spectra of 2b . | S28 |
| 15 | ¹ H and ¹³ C-NMR spectra of 3a . | S29 |
| 16 | ¹ H and ¹³ C-NMR spectra of 4a . | S30 |
| 17 | ¹ H and ¹³ C-NMR spectra of D1 . | S31 |
| 18 | ¹ H and ¹³ C-NMR spectra of D2 . | S32 |
| 19 | ¹ H and ¹³ C-NMR spectra of D3 . | S33 |
| 20 | ¹ H and ¹³ C-NMR spectra of Q1 . | S34 |
| 21 | ¹ H and ¹³ C-NMR spectra of Q2 . | S35 |
| 22 | ¹ H and ¹³ C-NMR spectra of Q3 . | S36 |

List of Tables

| | | |
|---|---|-----|
| 1 | Properties of Solvents used for Solvatochromism | S3 |
| 2 | Oxidation and reduction potentials | S10 |
| 3 | Solvatochromic fitting parameters | S12 |
| 4 | D -series fluorescence lifetimes | S17 |
| 5 | A and DCA fluorescence lifetimes | S18 |
| 6 | Q -series fluorescence lifetimes | S18 |

1 Materials

1.1 Photophysics and Electrochemistry

Cyclohexane (CX, Rotisolv, HPL), *n*-butyl ether (BE, Acros, 99 + % ExtraDry), propylene carbonate (PC, Acros, 99.5%) and tetrahydrofuran (TH, Rotidry, 99.9%, ≤ 50 ppm H₂O) were used as received for the photophysical measurements.

Table S 1: Dielectric properties (ϵ , n) and functions, $f(\epsilon)$, $f(n^2)$, of the solvents used for the photophysical investigation at 20 °C.

| Solvent | ϵ | n | $f(\epsilon)$ | $f(n^2)$ |
|----------------------------|------------|-------|---------------|----------|
| cyclohexane (CX) | 2.02 | 1.426 | 0.405 | 0.408 |
| <i>n</i> -butyl ether (BE) | 3.08 | 1.397 | 0.581 | 0.388 |
| tetrahydrofuran (TH) | 7.58 | 1.405 | 0.814 | 0.394 |
| propylene carbonate (PC) | 64.9 | 1.419 | 0.977 | 0.403 |

1.2 Synthesis

Reagents and solvents for the synthesis were purchased from commercial suppliers. Anhydrous solvents were prepared by filtration through drying columns (CH₂Cl₂, tetrahydrofuran (TH)) or used as received from suppliers (acetone, dimethylformamide (DMF), acetonitrile). Sodium hydride (60% suspension in oil) was rigorously stirred in petroleum ether for 15 min, filtered off, and dried in vacuo prior to use to remove the oil. 4-Ethynylanisole for Sonogashira coupling was prepared from 4-bromoanisole by coupling with trimethylsilylacetylene and subsequent deprotection using standard procedures.

2 Experimental Methods

2.1 NMR Spectroscopy

NMR spectra were recorded at 600 MHz for ¹H and 151 MHz for ¹³C on a Bruker Avance III HD spectrometer. ¹H-NMR signals were assigned as suggested by MestReNova (12.0.1- 20560). For ¹³C-NMR signals, the number of attached protons (C, CH, CH₃) was assigned by attached proton test (APT) experiments.

2.2 Electrochemistry

Samples were dissolved in acetonitrile with 0.1 M TBAPF₆ as electrolyte. All solutions were prepared in a glove-box under an Argon atmosphere, which had been dried with CaCl₂ and Na-chips to remove water and oxygen. Cyclic voltammograms were measured with a three-(micro)electrode system consisting of a silver working electrode ($\varnothing = 100 \mu\text{m}$), a tungsten reference electrode and a platinum counter electrode. Referencing was performed versus the ferrocene / ferrocenium couple (0.38 V vs. SCE),¹ which was measured in every sample by dropwise addition of a 15 mM ferrocene stock solution after the measurements. The redox potentials were estimated by choosing the maxima of the first derivative of the corresponding cyclovoltammograms (see the SI).

2.3 One-Photon (1P) Spectroscopy

A Cary 50 spectrometer and a FluoroMax-4 from Jobin-Yvon were used for steady-state absorption and emission / excitation measurements, respectively. Emission spectra were corrected using a set of secondary emissive standards.² Samples were prepared from concentrated ($c \approx 1-10$ mM)

stock solutions in dichloromethane or chloroform and diluted to the concentrations of interest using Hamilton syringes. Measurements were carried out in 1 cm quartz cuvettes at concentrations of maximum 20 μ M.

Absorption spectra for the determination of the extinction coefficient were measured on the freshly prepared samples. Samples for the determination of the fluorescence quantum yields were bubbled with nitrogen during 10 min and the absorption and emission spectra were measured. To reduce the error on the absorption terms in eq. (S1) samples with an absorbance at the excitation wavelength around 0.1-0.2 were used. In order to correct for the resulting distortions due to fluorescence reabsorption we proceeded as follows: The emission spectrum for a strongly dilute sample was used as correct lineshape function, unbiased by reabsorption. This lineshape function was then matched with the emission spectrum of the more concentrated sample in the wavelength range where reabsorption is negligible. The so-corrected emission spectra (free of any reabsorption) were further used.

For all samples fluorescence excitation spectra and absorption spectra were identical. Fluorescence from a minor impurity was only observable for **D3** and **Q3** at the blue edge of emission in the most polar solvent (PC), i.e. were basically no emission from the sample of interest was observed.

Fluorescence quantum yields were measured relative to Rhodamine 6G in methanol ($\phi_r = 0.93$)³ and calculated according to

$$\phi_s = \phi_r \left(\frac{n_s^2}{n_r^2} \right) \left(\frac{I_s}{I_r} \right) \left(\frac{A_r \cdot 10^{-d_{\text{eff}} \cdot A_r}}{A_s \cdot 10^{-d_{\text{eff}} \cdot A_s}} \right) \quad (\text{S1})$$

where n_x is the solvent refractive index, I_x is the integrated emission intensity, A_x is the absorbance of sample x at its excitation wavelength and d_{eff} is the effective distance from the cuvette excitation window to the point at which the luminescence is observed and which has been determined experimentally as proposed in reference 4.

In order to allow for a more reliable way of extracting the transition dipole moments, either for overlapping transitions in the absorption spectra or for emission spectra exceeding the experimentally available range, we adopted an approach outlined in ref. 5. In brief, we fit empirical lineshape functions, based on a displaced harmonic oscillator model, to the experimental absorption and emission spectra, $E_x(\tilde{\nu})$:

$$E_x(\tilde{\nu}) \propto \tilde{\nu}^i \sum_{n=0}^{n_{\text{max}}} \frac{S_x^n e^{-S_x}}{n!} \exp \left(\frac{-(h\tilde{\nu}_{0x} \pm n\hbar\omega_x - h\tilde{\nu})^2}{2\sigma_x^2} \right) \quad (\text{S2})$$

Here $i = 1, 3$ for absorption and emission, respectively. S_x , $\tilde{\nu}_{0x}$, ω_x and σ_x are the Huang-Rhys factor, the 0-0 vibronic transition energy, the coupling vibrational frequency and the width of each vibronic transition for $x \in \{\text{a}, \text{f}\}$ (absorption (+) and fluorescence (-)).

Transition dipole moments for absorption, M_a , and emission, M_f , were calculated according to ref. 6

$$M_a = 9.584 \cdot 10^{-2} \left(\frac{n}{f_n^2} \int_{10} \frac{\varepsilon(\tilde{\nu})}{\tilde{\nu}} d\tilde{\nu} \right)^{1/2}, \quad (\text{S3a})$$

$$M_f = 1785.7 \left(\frac{\phi_f}{\tau_f} \frac{1}{n f_n^2} \frac{\int I(\tilde{\nu}) \tilde{\nu}^{-3} d\tilde{\nu}}{\int I(\tilde{\nu}) d\tilde{\nu}} \right)^{1/2}, \quad (\text{S3b})$$

using the empty spherical cavity model for $f_n = \frac{3n^2}{2n^2 + 1}$.⁷ Note, that for M_a the integral has to be restricted to the $S_1 \leftarrow S_0$ band.

2.4 Time-Resolved Fluorescence

Fluorescence dynamics on the nanosecond time-scale were measured using a home-built time-correlated single photon counting (TCSPC) setup described in the supplementary material of

ref. 8. Excitation was performed at 395 nm using ~ 60 ps pulses at 5 MHz produced by a laser diode (Picoquant, LDH-P-C 400b). The full width at half maximum (FWHM) of the instrument response function (IRF) was around 200 ps. Fluorescence lifetimes for all samples were recorded in the blue and red of the corresponding emission spectra. The non-radiative rate constant, k_{nr} , is obtained from the lifetime, τ_{f} , and quantum yield, ϕ_{f} , measurements as follows:

$$k_{\text{nr}} = (1 - \phi_{\text{f}}) / \tau_{\text{f}} \quad (\text{S4})$$

2.5 Two-Photon (2P) Spectroscopy

2P cross sections were determined via 2P excitation spectra using a set-up similar to the one described in refs. 9,10. In detail, the output of a TOPAS-Prime in combination with a NirUVis frequency mixer (both from Light Conversion), which are themselves seeded by the output of an amplified femtosecond laser system (Spectra Physics, Spitfire, 1 kHz, 100 fs) was used as excitation source. The excitation intensity is adjusted using a combination of a broadband zero-order halfwaveplate and a Glan-Taylor polarizer, and the polarization set to vertical. The beam is slightly focused by a ($f = 20$ cm) lens, which is placed 14 cm before the sample. The pump power is monitored using a powermeter (Thorlabs PM100A) equipped with a photodiode power sensor (Thorlabs S120VC) behind the sample. The fluorescence is focused onto the entrance slit of a monochromator (0.25 m Cornerstone, Oriel, grating 74166 Newport) equipped with a multi-pixel photon-counter avalanche photodiode detector (Hamamatsu S-10362-11-050U) using a spherical mirror ($\varnothing = 75$ mm, $f = 150$ mm). The output signal is preamplified (SR240, Stanford Research Systems), processed with a gated boxcar-integrator and averager module (SR250, SRS), digitized (SR245, SRS) and recorded on a computer.

The 2P cross section at a given wavelength, $\sigma^{2\text{P}}(\lambda)$, was calculated as follows⁹

$$\sigma_{\text{s}}^{2\text{P}}(\lambda) = \frac{I_{\text{s}}(\lambda, \lambda_{\text{obs,s}}) \cdot c_{\text{r}} \cdot \phi'_{\text{r}}(\lambda_{\text{obs,r}})}{I_{\text{r}}(\lambda, \lambda_{\text{obs,r}}) \cdot c_{\text{s}} \cdot \phi'_{\text{s}}(\lambda_{\text{obs,s}})} \sigma_{\text{r}}^{2\text{P}}(\lambda) \quad (\text{S5})$$

Here $I_x(\lambda, \lambda_{\text{obs}})$ is the (two-photon induced) background-corrected fluorescence intensity at excitation wavelength λ and observation wavelength λ_{obs} for either sample or reference ($x \in \{\text{s}, \text{r}\}$). c_x and $\phi'_x(\lambda_{\text{obs},x})$ are the concentration and differential fluorescence quantum yield (at the observation wavelength) of sample and reference. Rhodamine 6G in methanol ($A_{\text{max}} = 0.2$, $\epsilon_{\text{max}} = 10.5 \cdot 10^4 \text{ M}^{-1} \text{ cm}^{-1}$ taken from ref. 11) was used as reference.¹²

2.6 Quantum Chemical Calculations

2.6.1 Computational Details

The molecular geometries were optimised with density functional theory using the PBE0 hybrid functional¹³ and Ahlrichs' TZVP basis set.¹⁴ Excited-state computations were performed using the wavefunction-based ab initio algebraic diagrammatic construction (ADC) method¹⁵ applying the resolution-of-the-identity approximation for the two-electron integrals. The excited-state wavefunctions were further characterised by an analysis of the one-electron transition density matrix,^{16,17} to decompose the excitation into local excitations on the individual parts as well as charge transfer contributions. Two-photon-absorption cross sections^{18,19} were computed using the formalism described below. All computations were performed using a developmental version of Q-Chem 5.0.0.²⁰

2.6.2 Integrated 1P absorption cross section

The integrated OPA cross section, $\tau^{1\text{P}}$, can be obtained from the calculated absorption transition dipole moments, $M_{\text{a},i}$, recasting eq. (S3a) as

$$\int \frac{\epsilon(\tilde{\nu})}{\tilde{\nu}} d\tilde{\nu} = 108.87 M_{\text{a}}^2 = \tau^{1\text{P}} \quad (\text{S6})$$

The numerical prefactor (108.87) is applicable when M_a is given in Debye and yields τ^{1P} in $M^{-1}cm^{-1}$. Here, the refractive index dependent contributions (present in eq. (S3a)) have been omitted, i.e. the gas-phase value is calculated.

2.6.3 Integrated 2P absorption cross section

We compute the 2P absorption properties at the ADC level of theory as described in refs 18,19. The two-photon transition moment tensor for two resonant photons of equal energy is given as

$$\mathbf{S} = \frac{1}{e^2} \sum_{n \neq 0} \frac{\vec{\mu}_{0n} \vec{\mu}'_{nf}{}^T}{\omega_n - \omega_f/2} + \frac{\vec{\mu}'_{nf} \vec{\mu}_{0n}{}^T}{\omega_n - \omega_f/2} \quad (S7)$$

Here, ω_a is the transition frequency of state a , $\vec{\mu}_{ab}$ denotes the (transition) dipole moment vector between states a and b , and $\vec{\mu}'_{nf}$ is a shifted dipole moment vector defined as

$$\vec{\mu}'_{nf} = \vec{\mu}_{nf} - \vec{\mu}_{00} \delta_{nf} \quad (S8)$$

As opposed to refs 18,19, we formally divide the expression in eq. (S7) by the square of the unit charge e , which means that \mathbf{S} has the dimension of a squared length multiplied by time. In atomic units, this is Bohr radius squared times the atomic time unit (a.t.u.), [$\text{Bohr}^2 \text{ a.t.u.}$]. The two-photon absorption strength is given as

$$\delta^{2P} = \frac{F \text{tr}(\mathbf{S})^2 + G \text{tr}(\mathbf{S}\mathbf{S}^T) + H \text{tr}(\mathbf{S}\mathbf{S})}{30} \quad (S9)$$

where in the case of parallel linearly polarized light the coefficients are $F = G = H = 2$. The dimension of δ^{2P} as defined here is the fourth power of length multiplied by time squared, e.g. in atomic units [$\text{Bohr}^4 \text{ a.t.u.}^2$].

To compute the macroscopic cross-section, we follow refs 21,22 and obtain the following equation

$$\sigma^{2P} = 4\pi^3 \alpha^2 \omega^2 \delta^{2P} g(2\omega, \omega_f, \Gamma), \quad (S10)$$

where α is the fine-structure constant, ω is the photon frequency, and g is a normalized line-shape function. Note that this expression holds independent of the set of units used. When evaluated in terms of atomic units, it is equivalent to eq. (1) of ref. 21. To compute an integrated cross-section, we divide the above equation by 2ω , fix the photon frequency on the right-hand-side as $2\omega = \omega_f$ and integrate over $d2\omega$ to obtain

$$\int \frac{\sigma^{2P}(\omega)}{2\omega} d2\omega = \pi^3 \alpha^2 \omega_f \delta^{2P} \int g(2\omega, \omega_f, \Gamma) d2\omega \quad (S11)$$

As a final step, we multiply the left side by an enhancement factor F and cancel out the factor 2, and we eliminate the integral over the normalized line-shape function on the r.h.s.

$$F \int \frac{\sigma^{2P}(\omega)}{\omega} d\omega = \pi^3 \alpha^2 \omega_f \delta^{2P} = \tau^{2P} \quad (S12)$$

This is the final working equation, we use to compare theory and experiment. The left side is entirely experimental, the right side entirely computational. By using the identities $\epsilon_0 \mu_0 = 1/c^2$ and $\frac{1}{\epsilon_0 \hbar c} = \frac{4\pi\alpha}{e^2}$, it can be worked out that the prefactor in eq. (S12) is the same as the one used in eq. (3) of ref. 23. Eq. (S12) holds independently of the set of units used. Practically, the results are usually reported in GM, i.e. $10^{-50} \text{cm}^4 \text{s photon}^{-1}$. For the conversion, it has to be first realized that one atomic unit (a.u.) of two-photon absorption is given as [$\text{Bohr}^4 \text{ a.t.u. photon}^{-1}$], which is equivalent to 1.897 GM. Combining this prefactor of Eq. (S12) with the unit conversion one obtains a value of $\pi^3 \alpha^2 = 0.0031318 \text{ GM/a.u.}$ that has to be inserted into the

right-hand-side of eq. (S12) when ω_f and δ^{2P} are both given in atomic units. As a final note, we want to point out that in the Q-Chem version used the factor 1/30 is missing in the definition of δ^{2P} meaning that this factor has to be included in the conversion, as well.

The conversion factor between the integrated cross-section τ^{2P} and the cross-section at the absorption maximum is

$$\sigma_{\max}^{2P} = \frac{\omega_f}{\Gamma} \sqrt{\frac{\ln(2)}{\pi}} \tau^{2P} \quad (\text{S13})$$

assuming a Gaussian line shape with Γ as HWHM.

3 Synthesis

3.1 Methoxy-substituted anthraquinones 2a-b

2a: Synthesis carried out adapting and scaling-up a published procedure.²⁴ Starting material **1a** (1.12 g, 5.0 mmol, 1.0 equiv) was dissolved in 50 mL dry DMF (0.1 M) in a 100 mL three-necked round bottom flask equipped with a drying tube (filled with CaCl_2 beads). Sodium hydride (240 mg, 10 mmol, 2.0 equiv) was then added to the stirred solution. After 15 min, iodomethane (7.10 g, 50 mmol, 10 equiv) dissolved in 25 mL methyl tert-butyl ether (MTBE, 2.0 M) was added and the reaction stirred at room temperature for 18 h. The resulting brown suspension was then slowly poured into 150 mL ice water; the solid was filtered off and washed with 100 mL cold methanol. The crude product was dissolved in CH_2Cl_2 and purified by filtration through a pad of silica (using CH_2Cl_2 as eluent). Evaporation of the solvent afforded target compound **2a** (956 mg, 4.0 mmol, 80%) as slightly green solid. ^1H NMR (600 MHz, CDCl_3): δ = 8.33 – 8.28 (m, 2H), 8.27 (d, J = 8.7 Hz, 1H), 7.82 – 7.75 (m, 2H), 7.74 (d, J = 2.7 Hz, 1H), 7.28 (dd, J = 8.6, 2.7 Hz, 1H), 3.99 (s, 3H). ^{13}C NMR (151 MHz, CDCl_3): δ = 183.5 (C), 182.3 (C), 164.5 (C), 135.7 (C), 134.3 (CH), 133.8 (CH), 133.8 (C), 133.7 (C), 129.9 (CH), 127.3 (CH), 127.3 (C), 121.4 (CH), 110.1 (CH), 56.1 (CH_3) ppm. See Figure S13.

2b: Synthesis carried out adapting a procedure previously used for the synthesis of 1,8-dimethoxyanthraquinone.²⁵ Subjecting starting material **1b** (3.60 g, 15.0 mmol) to this procedure afforded target compound **2b** (3.21 g, 12.0 mmol, 80%) as light yellow solid. In contrast to the published procedure, purification was done by flash chromatography (using CH_2Cl_2 as eluent). ^1H NMR (600 MHz, CDCl_3): δ = 8.24 (d, J = 8.6 Hz, 2H), 7.73 (d, J = 2.7 Hz, 2H), 7.24 (dd, J = 8.6, 2.7 Hz, 2H), 3.99 (s, 6H) ppm. ^{13}C NMR (151 MHz, CDCl_3): δ = 182.4 (C), 164.6 (C), 136.0 (C), 129.9 (CH), 127.3 (C), 120.8 (CH), 110.1 (CH), 56.1 (CH_3) ppm. See Figure S14.

3.2 General procedure for the synthesis of methoxy-substituted DCAs D1 and Q1

An argon flushed reaction vial equipped with a septum was charged with trimethylsilyl cyanide (TMSCN, 0.14 mL, 109 mg, 1.1 mmol, 2.2 equiv). $n\text{-BuLi}$ (0.02 mL, 0.05 mmol, 0.1 eq, 2.2 M in hexanes) was added carefully at room temperature under rigorous stirring. After 15 min, the resulting suspension was transferred to the starting material **2a/2b** (0.5 mmol, 1.0 equiv), which was precooled to 0°C in another argon flushed reaction vial equipped with a septum. Dry DMF (0.25 mL) was used to fully transfer remaining residues. The resulting solution was stirred at 0°C overnight. Dry CH_2Cl_2 (1.5 mL) was then added slowly. Subsequently, PBr_3 (0.06 mL, 162 mg, 0.6 mmol, 1.2 equiv) was added, the septum was replaced by a sealed cap, and the mixture again stirred at 0°C overnight. For work-up, the reaction was warmed to room temperature and directly filtered through a thick pad of silica (conditioned with CH_2Cl_2) using CH_2Cl_2 as eluent. After evaporation of the solvent, the crude product was further purified by column chromatography (petroleum ether:toluene) to yield target compound **D1/Q1**. Despite high purity, the target compounds were further purified by recrystallization from acetonitrile prior to in-depth characterization.

D1: Synthesis following the general procedure using starting material **2a** (119 mg, 0.5 mmol). Column chromatography (petroleum ether:toluene 1 : 1 \rightarrow 1 : 2) afforded target compound **D1** (32 mg, 0.12 mmol, 25%) as bright yellow solid. ^1H NMR (600 MHz, CDCl_3): δ = 8.50 – 8.43 (m, 2H), 8.40 (d, J = 9.3 Hz, 1H), 7.86 – 7.75 (m, 2H), 7.62 (d, J = 2.4 Hz, 1H), 7.49 (dd, J = 9.3, 2.4 Hz, 1H), 4.08 (s, 3H) ppm. ^{13}C NMR (151 MHz, CDCl_3): δ = 160.8 (C), 134.5 (C), 132.6 (C), 130.4 (C), 130.0 (CH), 129.0 (C), 128.8 (CH), 128.0 (CH), 126.4 (CH), 125.7 (CH), 125.4 (CH), 116.6 (C), 116.1 (C), 111.6 (C), 108.8 (C), 101.9 (CH), 56.1 (CH_3) ppm. See Figure S17. HRMS (EI/TOF) m/z : $[\text{M}]^+$ Calcd for $\text{C}_{17}\text{H}_{10}\text{N}_2\text{O}$ 258.0788; Found 258.0794.

Q1: Synthesis following the general procedure using starting material **2b** (134 mg, 0.5 mmol). Column chromatography (petroleum ether:toluene 1:2) afforded target compound **D2** (39 mg, 0.14 mmol, 27%) as bright yellow solid. ^1H NMR (600 MHz, CDCl_3): δ = 8.33 (d, J = 9.3 Hz, 2H), 7.58 (d, J = 2.5 Hz, 2H), 7.47 (dd, J = 9.3, 2.5 Hz, 2H), 4.06 (s, 6H) ppm. ^{13}C NMR (151 MHz, CDCl_3): δ = 159.9 (C), 132.5 (C), 129.2 (C), 127.4 (CH), 125.1 (CH), 116.6 (C), 109.0 (C), 102.3 (CH), 56.0 (CH_3) ppm. See Figure S20. HRMS (EI/TOF) m/z : $[\text{M}]^+$ Calcd. for $\text{C}_{18}\text{H}_{12}\text{N}_2\text{O}_2$ 288.0893; Found 288.0900.

3.3 Synthesis of anthraquinone triflates **3a-b**

3a: Synthesis carried out following a published procedure.²⁶ ^1H NMR (600 MHz, CDCl_3): δ = 8.45 (d, J = 8.5 Hz, 1H), 8.37 – 8.31 (m, 2H), 8.19 (d, J = 2.6 Hz, 1H), 7.90 – 7.82 (m, 2H), 7.69 (dd, J = 8.6, 2.6 Hz, 1H) ppm. ^{13}C NMR (151 MHz, CDCl_3): δ = 181.7 (C), 181.5 (C), 153.4 (C), 135.9 (C), 134.9 (CH), 134.8 (CH), 133.4 (C), 133.2 (C), 133.1 (C), 130.5 (CH), 127.7 (CH), 127.7 (CH), 127.0 (CH), 120.1 (CH), 118.8 (CF_3 , q, J = 320.9 Hz) ppm. See Figure S15.

3b: Synthesis carried out following a published procedure.²⁷

3.4 Synthesis of DCA triflates **4a-b**

4a: An argon flushed reaction vial equipped with a septum was charged with TMSCN (0.14 mL, 109 mg, 1.1 mmol, 2.2 equiv). $n\text{-BuLi}$ (0.02 mL, 0.05 mmol, 0.1 eq, 2.2 M in hexanes) was added carefully at room temperature under rigorous stirring. After 15 min, the resulting suspension was transferred to the starting material **3a** (178 mg, 1.0 eq, 0.5 mmol) in another reaction vial equipped with a septum. Dry DMF (0.25 mL) was used to fully transfer remaining residues. The resulting red brown solution stirred at room temperature for 3 h. Dry acetonitrile (1.5 mL) and PBr_3 (0.06 mL, 162 mg, 0.6 mmol, 1.2 equiv) were then added, the septum was replaced by a sealed cap, and the reaction was heated to 50°C overnight. The reaction was then cooled to room temperature, diluted with CH_2Cl_2 (4 mL), and directly filtered through a thick pad of silica (conditioned with CH_2Cl_2 and a few drops of acetonitrile) using CH_2Cl_2 as eluent. After evaporation of the solvent, the crude product was further purified by column chromatography (petroleum ether: CH_2Cl_2 9:1 – 7:3), which afforded **4a** (49 mg, 0.13 mmol, 26%) as bright yellow solid. The low yield can be attributed to the poor separation during column chromatography. ^1H NMR (600 MHz, CD_2Cl_2): δ = 8.66 (dd, J = 9.4, 0.6 Hz, 1H), 8.59 – 8.51 (m, 2H), 8.43 (dd, J = 2.4, 0.6 Hz, 1H), 7.98 – 7.91 (m, 2H), 7.77 (dd, J = 9.4, 2.4 Hz, 1H) ppm. ^{13}C NMR (151 MHz, CD_2Cl_2): δ = 150.0 (C), 133.4 (C), 133.2 (C), 132.3 (C), 131.5 (CH), 131.3 (CH), 131.0 (C), 130.3 (CH), 126.8 (CH), 126.6 (CH), 124.5 (CH), 119.3 (CF_3 , q, J = 320.5 Hz), 118.2 (CH), 115.8 (C), 115.7 (C), 112.9 (C), 112.7 (C) ppm. See Figure S16. HRMS (EI/TOF) m/z : $[\text{M}]^+$ Calcd. for $\text{C}_{17}\text{H}_7\text{F}_3\text{N}_2\text{O}_2$ 376.0124; Found 376.0127.

4b: Synthesis carried out following a published protocol.²⁸

3.5 Synthesis of 4-methoxyphenyl-substituted DCAs **D2** and **Q2**

D2: A reaction vial equipped with a septum was charged with starting material **4a** (75 mg, 0.2 mmol, 1.0 equiv) and 4-methoxyphenylboronic acid (76 mg, 0.50 mmol, 2.5 equiv). After flushing with argon, TH (4 mL, purged with argon) was added and the mixture was heated to 70°C

until the solid was fully dissolved. 2.0 M aqueous K₂CO₃ solution (0.5 mL, 1.0 mmol, 5.0 equiv, purged with argon) and Pd(PPh₃)₄ (6 mg, 0.005 mmol, 0.025 equiv) were then added under a stream of argon. The reaction stirred at 70°C for 90 min and was then cooled to room temperature. The dark orange solution was poured into 100 mL water and extracted three times with CH₂Cl₂. The combined organic layers were dried over Na₂SO₄ and the solvent was removed in vacuo. The yellow residue was dissolved in CH₂Cl₂, filtered through a thick pad of silica (conditioned with CH₂Cl₂) using approx. 500 mL CH₂Cl₂ as eluent, and evaporated again in vacuo. The solid residue was recrystallized by dissolving in 8 mL boiling toluene and adding the same amount of isopropyl alcohol. Target compound **D2** (53 mg, 0.16 mmol, 79%) was obtained as yellow solid. ¹H NMR (600 MHz, CD₂Cl₂): δ = 8.61 (dd, *J* = 1.8, 0.7 Hz, 1H), 8.56 (dd, *J* = 9.0, 0.7 Hz, 1H), 8.54 - 8.47 (m, 2H), 8.14 (dd, *J* = 9.0, 1.8 Hz, 1H), 7.89 - 7.80 (m, 4H), 7.14 - 7.07 (m, 2H), 3.90 (s, 3H) ppm. ¹³C NMR (151 MHz, CD₂Cl₂): δ = 161.1 (C), 142.3 (C), 133.2 (C), 133.0 (C), 132.2 (C), 131.8 (C), 131.6 (C), 130.3 (CH), 130.3 (CH), 130.0 (CH), 129.4 (CH), 127.1 (CH), 126.6 (CH), 126.5 (CH), 122.3 (CH), 116.6 (C), 116.4 (C), 115.2 (CH), 111.9 (C), 111.5 (C), 56.0 (CH₃) ppm. See Figure S18. HRMS (EI/TOF) *m/z*: [M]⁺ Calcd. for C₂₃H₁₄N₂O 334.1101; Found 334.1103.

Q2: A reaction vial equipped with a septum was charged with starting material **4b** (105 mg, 0.2 mmol, 1.0 equiv) and 4-methoxyphenylboronic acid (91 mg, 0.60 mmol, 3.0 equiv). After flushing with argon, TH (4 mL, purged with argon) was added and the mixture was heated to 70°C until the solid was fully dissolved. 2.0 M aqueous K₂CO₃ solution (0.5 mL, 1.0 mmol, 5.0 equiv, purged with argon) and Pd(PPh₃)₄ (12 mg, 0.01 mmol, 0.05 equiv) were then added under a stream of argon. The reaction stirred at 70°C for 3 h and was then cooled to room temperature. The red solid, which precipitated from the red brown solution already during the reaction, was filtered off and washed with water and CH₂Cl₂. Recrystallization from approx. 200 mL 1,2-dichloroethane afforded target compound **Q2** (62 mg, 0.14 mmol, 70%) as bright orange solid. ¹H NMR (600 MHz, CD₂Cl₂): δ = 8.61 (d, *J* = 1.7 Hz, 2H), 8.55 (d, *J* = 9.0 Hz, 2H), 8.14 (dd, *J* = 8.9, 1.8 Hz, 2H), 7.87 - 7.81 (m, 4H), 7.13 - 7.08 (m, 4H), 3.90 (s, 6H) ppm. ¹³C NMR (151 MHz, CD₂Cl₂): δ = 161.1 (C), 142.0 (C), 132.8 (C), 132.2 (C), 131.7 (C), 130.3 (CH), 129.3 (CH), 127.1 (CH), 122.4 (CH), 116.6 (C), 115.2 (CH), 111.3 (C), 56.0 (CH₃) ppm. See Figure S21. HRMS (APCI/Orbitrap) *m/z*: [M]⁺ Calcd. for C₃₀H₂₀N₂O₂ 440.1519; Found 440.1519.

3.6 Synthesis of (4-methoxyphenyl)ethynyl-substituted DCAs D3 and Q3

D3: A reaction vial equipped with a septum was charged with starting material **4a** (75 mg, 0.2 mmol, 1.0 equiv), PdCl₂(PPh₃)₂ (3.5 mg, 5 μmol, 0.025 equiv), and CuI (1.0 mg, 5 μmol, 0.025 equiv). The vial was flushed with argon before TH : diisopropylamine (5:1, 4.8 mL, purged with argon) was added. The yellow suspension stirred at room temperature for 10 min, 4-ethynylanisole (33 mg, 0.25 mmol, 1.25 equiv) was then added via the septum, and the reaction was heated to 60°C for 3 h. After cooling to room temperature, the mixture was poured into 40 mL saturated aqueous NH₄Cl solution and extracted three times with 40 mL CH₂Cl₂. The combined organic layers were dried over Na₂SO₄ and the solvent was evaporated in vacuo. The brown solid residue was recrystallized by dissolving in 1.5 mL boiling toluene and then adding the same amount of isopropyl alcohol. Target compound **D3** (48 mg, 0.13 mmol, 67%) was obtained as bright orange solid. ¹H NMR (600 MHz, CD₂Cl₂): δ = 8.64 (dd, *J* = 1.5, 0.8 Hz, 1H), 8.54 - 8.49 (m, 2H), 8.47 (dd, *J* = 9.0, 0.8 Hz, 1H), 7.91 - 7.84 (m, 3H), 7.62 - 7.57 (m, 2H), 6.98 - 6.93 (m, 2H), 3.86 (s, 3H) ppm. ¹³C NMR (151 MHz, CD₂Cl₂): δ = 161.1 (C), 134.1 (CH), 133.0 (C), 132.6 (CH), 132.6 (C), 132.5 (C), 131.7 (C), 130.6 (CH), 130.4 (CH), 128.7 (CH), 126.7 (CH), 126.7 (CH), 126.7 (CH), 126.0 (C), 116.3 (C), 116.2 (C), 114.8 (CH), 114.7 (C), 112.1 (C), 111.2 (C), 95.0 (C), 87.9 (C), 55.9 (CH₃) ppm. See Figure S19. HRMS (APCI/Orbitrap) *m/z*: [M]⁺ Calcd. for C₂₅H₁₄N₂O 358.1101; Found 358.1108.

Q3: A reaction vial equipped with a septum was charged with starting material **4b** (105 mg,

0.2 mmol, 1.0 equiv), PdCl₂(PPh₃)₂ (7 mg, 10 μmol, 0.05 equiv), and CuI (2 mg, 10 μmol, 0.05 equiv.). The vial was flushed with argon before TH : diisopropylamine (5:1, 4.8 mL, purged with argon) was added. The yellow suspension stirred at room temperature for 10 min, 4-ethynylanisole (66 mg, 0.5 mmol, 2.5 equiv) was then added via the septum, and the reaction was heated to 60°C for 3 h. After cooling to room temperature, the red solid, which precipitated already during the reaction, was separated from the solution by centrifugation. The solid was suspended in diethyl ether, separated again from the solvent by centrifugation, and dried in vacuo to yield target compound **Q3** (85 mg, 0.17 mmol, 87%) as red powder. ¹H NMR (600 MHz, CD₂Cl₂): δ = 8.62 (dd, *J* = 1.5, 0.8 Hz, 2H), 8.46 (dd, *J* = 8.9, 0.8 Hz, 2H), 7.90 (dd, *J* = 8.9, 1.5 Hz, 2H), 7.62 - 7.57 (m, 4H), 6.99 - 6.93 (m, 4H), 3.86 (s, 6H) ppm. ¹³C NMR (151 MHz, CD₂Cl₂): δ = 161.1 (C), 134.1 (CH), 132.9 (CH), 132.4 (C), 132.1 (C), 128.8 (CH), 126.7 (CH), 126.1 (C), 116.1 (C), 114.8 (CH), 114.7 (C), 111.2 (C), 95.3 (C), 88.0 (C), 56.0 (CH₃) ppm. See Figure S22. HRMS (APCI/Orbitrap) *m/z*: [M]⁺ Calcd. for C₃₄H₂₀N₂O₂ 488.1518; Found 488.1519.

4 Additional Experimental Results

4.1 Electrochemistry

Table S2: Oxidation, E^{ox} , and reduction potentials, E^{red} , of the collected samples, measured in acetonitrile containing 0.1 M TBA(PF₆) using cyclic voltammetry. The ferrocene / ferrocenium couple was used as internal reference. The potentials are given in V vs. SCE.

| | E_1^{ox} | E_2^{ox} | E_1^{red} | E_2^{red} | E_3^{red} |
|----------------------|-------------------|---------------------|----------------------|--------------------|--------------------|
| A^a | 1.09 | | −1.95 | | |
| DCA | 1.88 | | −0.95 | −1.65 | |
| D1 | 1.64 | (2.27) ^b | −1.03 | −1.69 | |
| D2 | 1.56 | 1.89 | −0.92 | −1.61 | |
| D3 | 1.48 | 1.93 | −0.87 | −1.54 | |
| Q1 | 1.51 | 2.17 | −0.89 | −1.09 | −1.69 |
| Q2 | 1.52 | | −0.70 | −0.92 | |
| Q3 | 1.50 | 1.86 | (−0.58) ^b | −0.75 | −1.34 |

^a taken from ref. 29

^b not unambiguously assignable

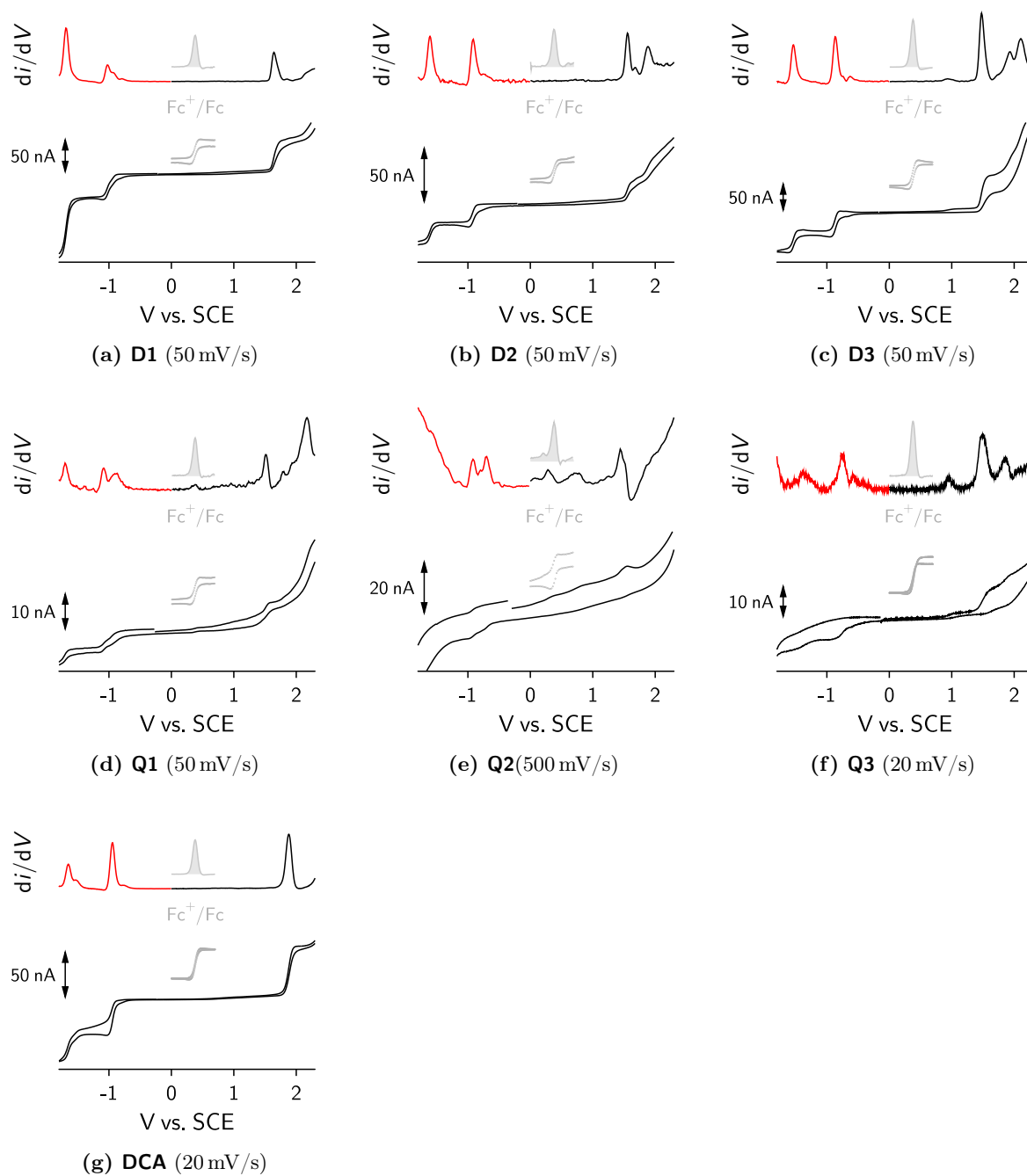


Figure S 1: Cyclic voltammograms (lower panels) of all samples in acetonitrile with 0.1 M TBAPF₆. In addition the first derivatives of the CVs are shown (upper panels), rendering the assignment of the half-wave potentials easier. The black line indicates the forward direction for oxidation while the red line is the forward direction for the reduction scan. The position of the ferrocene/ferrocenium couple, as measured in the corresponding sample, is shown as grey insets and has been used to reference vs. SCE.

4.2 Photophysics

4.2.1 Solvatochromism

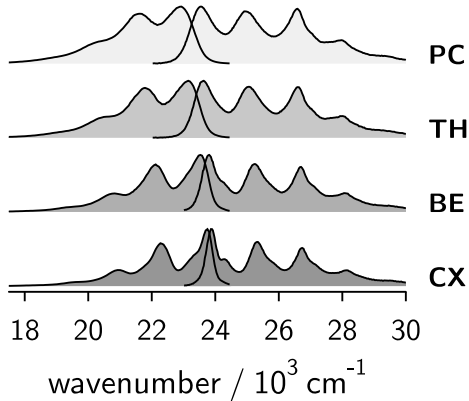


Figure S2: Solvent dependence of absorption and fluorescence of **DCA**.

Table S 3: Fitting parameters, A_i and B_i for the solvatochromic shifts ($1 \text{ kK} = 1000 \text{ cm}^{-1}$) in absorption and emission using eq. (2) and their estimated errors.^a Note, that A_x is not the gas-phase transition wavenumber. It is merely given to allow reconstruction of the values in the various solvents using eq. (2) and Fig. S4.

| | absorption ^b | | | fluorescence ^c | | |
|----------------------|-------------------------|---------------|-------|---------------------------|---------------|-------|
| | A_a (kK) | B_a (kK) | r^2 | A_f (kK) | B_f (kK) | r^2 |
| A^d | | −0.24 | | | −0.30 | |
| DCA | 24.13 | −0.62 | 0.97 | 24.35 | −1.45 | 1.00 |
| D1 | 22.92 | −0.38 | 0.95 | 21.67 | −2.61 | 0.99 |
| D2 | 22.37 | 0.00 | 1.00 | 22.93 | −7.53 | 0.99 |
| D3 | 21.58 | 0.72 | 0.99 | 24.47 | −10.91 | 0.97 |
| Q1 | 22.30 | −0.57 | 0.97 | 20.55 | −2.02 | 1.00 |
| Q2 | 21.51 | −0.60 | 0.99 | 21.54 | −5.46 | 0.95 |
| Q3 | 20.64 | 0.00 | 1.00 | 25.66 | −12.26 | 0.95 |

^a The error on A_x is 0.17 kK and the one on B is 0.23 kK, as determined using the method published by York et al.³⁰. For this purpose the standard errors on the experimental data were taken to be 0.1 kK, which is approximately twice the used bandpass of the spectrometers in the 400-800 nm range, while the error in the solvent polarity function was deemed negligibly small (using 0.0001).

^b the lowest energetic vibronic absorption band was used.

^c except for **DCA** (highest energy vibronic maximum) the center of gravity of the band was taken due to the significant changes in lineshape.

^d parameters taken from ref. 31.

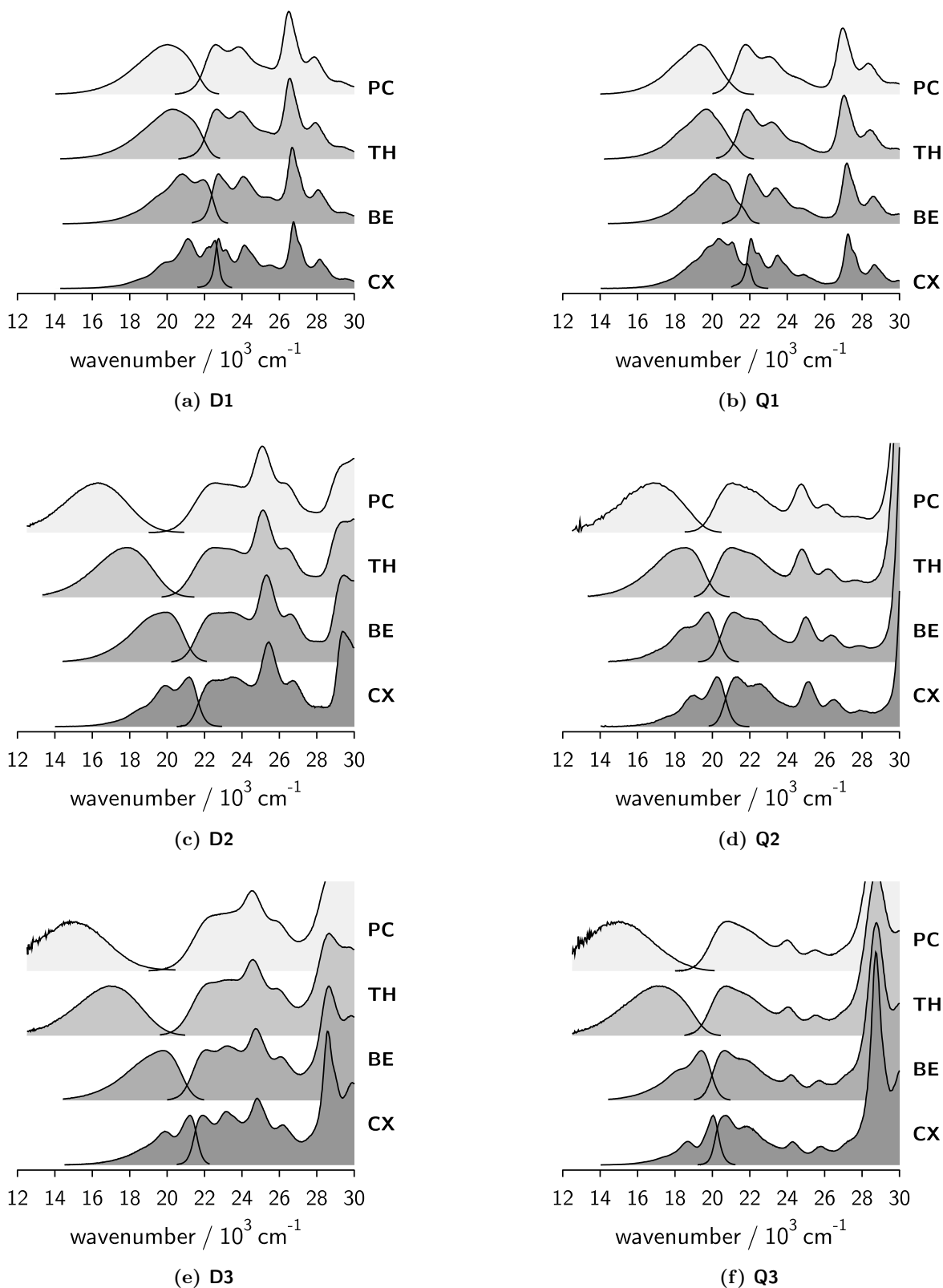


Figure S 3: Solvent dependence of absorption and emission spectra of **D** and **Q**-series. Absorption spectra of **Q2** (except for TH) are excitation spectra, due to the low solubility of the samples.

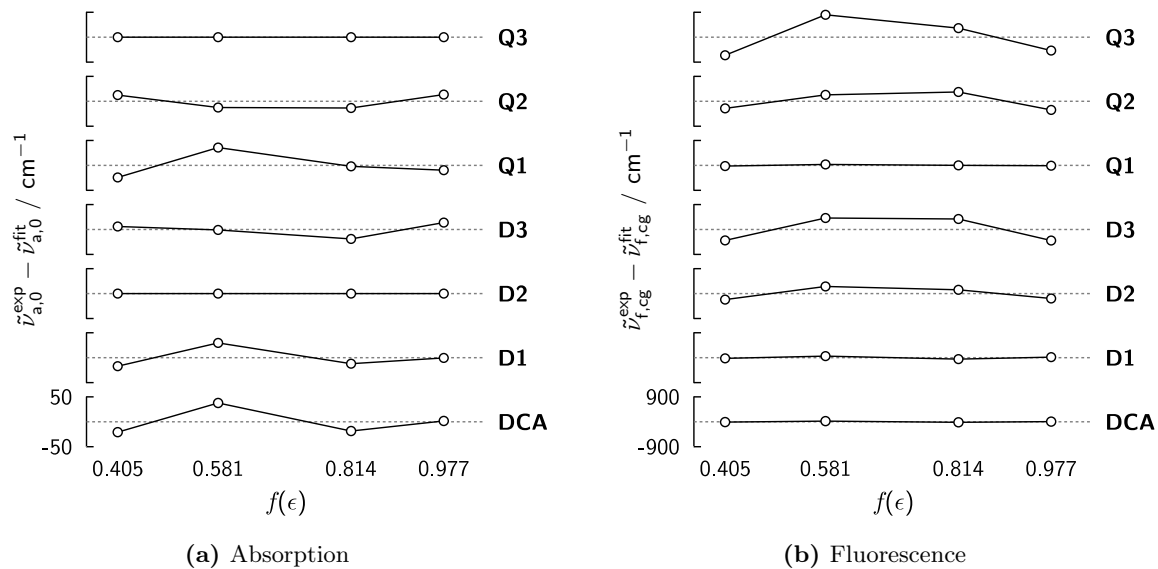


Figure S 4: Residuals of the linear fits (with parameter from Table S3) to the solvatochromic shifts of the lowest energetic absorption and emission band as a function of the solvent dipolarity function, $f(\epsilon)$.

4.2.2 Mirror Symmetry Relation

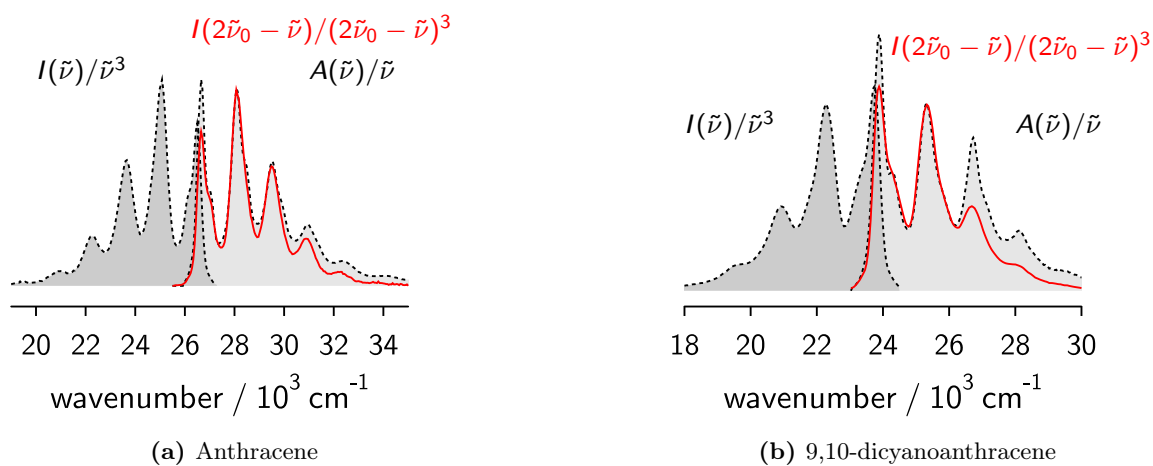


Figure S 5: Absorption (light grey), emission (dark grey) and mirrored (red line) emission spectra of **A** (a) and **DCA** (b) in cyclohexane in the transition dipole moment representation.

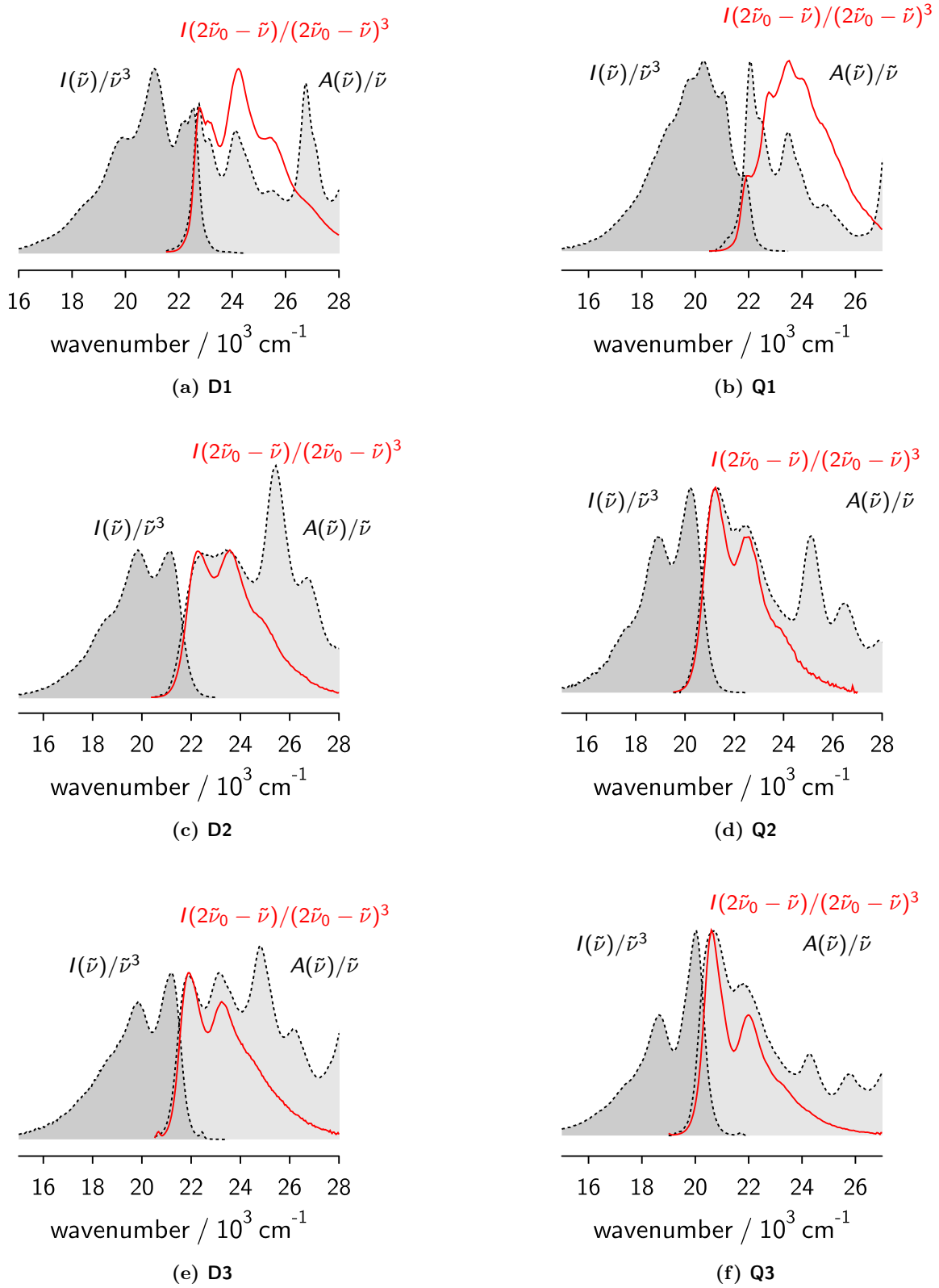


Figure S 6: Absorption (light grey), emission (dark grey) and mirrored (red line) emission spectra of **Ds** (left column) and **Qs** (right column) in cyclohexane in the transition dipole moment representation.

5 Effect of molecular size on fluorescence solvatochromism

Let's assume that the dipole moments of the ground, μ_g , and excited state, μ_e , grow with the cavity size, a . Not necessarily this increase ought to occur in a linear way. The slope of the fluorosolvatochromic plot (when solvents of identical refractive index are used) is given by:

$$B_f = -\frac{1}{a^3} \mu_e (\mu_e - \mu_g^{\text{FC}}). \quad (\text{S14})$$

Let's assume that $\mu_e = f(a)$ and investigate two different cases for the nature of the Franck-Condon ground state (FCGS):

- Case 1: the FCGS has the same nature as the excited state, therefore $\mu_g^{\text{FC}} = kf(a)$ with $0 < k < 1$.
- Case 2: the FCGS has a different nature than the excited state and $\mu_g^{\text{FC}} = k$ with $k > 0$.

Now let's see in each case what happens to the derivative of eq. (S14) to study the trends to be observed in the solvatochromism of molecules of increasing sizes.

Case 1

$$B_f = -\frac{1}{a^3} f(a) [f(a) - kf(a)] = \frac{1}{a^3} f^2(a) [k - 1] \quad (\text{S15})$$

$$\frac{\partial B_f}{\partial a} = \frac{f(a)(1-k)}{a^4} [3f(a) - 2af'(a)]. \quad (\text{S16})$$

$f(a)$ is always a growing and positive function, therefore the part outside the square brackets in eq. (S16) is always positive. The sign of the derivative of B_f depends only on the sign of the expression inside them.

If $f(a)$ is a linear function of a , then the expression inside the brackets is always positive, i.e. $3a - 2a$, and increasing the size of the cavity leads to smaller solvatochromic shifts.

If $f(a) \propto a^n$ with $n > 1$, then the sign depends on $3 - 2n$, so for values of n larger than 1.5 the trend inverts and increasing the size of the cavity leads to larger solvatochromic shifts.

Case 2

$$B_f = -\frac{1}{a^3} f(a) [f(a) - k] \quad (\text{S17})$$

$$\frac{\partial B_f}{\partial a} = \frac{1}{a^4} [3f^2(a) - 2af(a)f'(a) - 3f(a)k + af'(a)k]. \quad (\text{S18})$$

All the terms inside the brackets of eq. (S18) are positive under the conditions expressed above and in case 1: $f(a)$ is always a growing and positive function, therefore the part outside the square brackets is always positive and $k > 0$. Therefore in order to find the sign of the derivative one needs to determine the sign of the expression in square brackets. If $f(a) = a$, the sign of eq. (S18) comes from the difference $a - 2k$, such that if $k > a/2$ the slope is negative and the fluorescence solvatochromism increases with the length of the cavity.

For any other functional dependence of $f(a)$ things are more complicated, and there are ranges of values of k in which the trends are positive, other negatives and so on. For example for a quadratic dependence there is a region of values of k between 0 and $2/3$ in which the derivative of B_f is negative and outside it is always positive.

6 Time-resolved Emission Data

Table S 4: Fluorescence lifetimes of deoxygenated solutions of the **D**-series in various solvents at different observation wavelength.

| | solvent | λ_{obs} [nm] | τ_1 [ns] | A_2/A_1 | τ_2 [ns] | χ_r^2 |
|-----------|-----------------------|--------------------------------|------------------|-----------|------------------|------------|
| D1 | CX | 450 ^a | 16.2 | 4.0 | 11.4 | 1.03 |
| | | 467 | 16.3 | | | 1.02 |
| | | 488 | 15.9 | | | 0.97 |
| | | 500 | 15.4 | −0.6 | 13.2 | 1.00 |
| | | 520 ^a | 14.9(3) | −1.0 | 14.8(5) | 0.97 |
| | | 540 | 16.5 | −0.4 | 11.9 | 0.96 |
| | | 570 ^a | 14.7 | −1.0 | 14.6 | 1.05 |
| | | 590 | 16.2 | −0.6 | 12.7 | 0.98 |
| | BE TH ^b | 520 | 18.7 | | | 1.13 |
| | | 450 | 16.0 | | | 0.98 |
| | | 467 | 16.4 | | | 1.00 |
| | | 520 | 18.1 | | | 1.06 |
| | PC | 575 | 18.6 | | | 0.98 |
| | | 467 | 18.1 | | | 0.98 |
| | | 570 | 20.2 | | | 1.05 |
| D2 | CX | 467 | 5.1 | | | 1.10 |
| | | 570 | 5.5 | | | 1.06 |
| | BE | 467 | 7.8 | | | 1.12 |
| | | 570 | 7.9 | | | 1.04 |
| | TH | 488 | 12.5 | | | 1.01 |
| | | 570 | 12.6 | | | 1.06 |
| | | 635 | 12.6 | | | 1.10 |
| | PC | 540 | 8.9 | | | 1.07 |
| | | 670 | 8.9 | | | 1.00 |
| D3 | CX | 467 | 6.9 | | | 1.02 |
| | | 540 | 7.0 | | | 1.07 |
| | BE | 488 | 5.7 | | | 1.02 |
| | | 610 | 5.7 | | | 1.08 |
| | TH | 540 | 7.2 | | | 1.07 |
| | | 670 | 7.2 | | | 1.01 |
| | PC | 540 | 0.7 | | | 1.19 |
| | | 690 | 0.7 | | | 1.37 |

^a identical lifetimes for **D1** concentrations of $3 \cdot 10^{-6}$ and $2 \cdot 10^{-5}$ M.

^b maybe biexponential decays, though the already low χ_r^2 do not recommend it

Table S 5: Fluorescence lifetimes of deoxygenated solutions of **A** and **DCA** in various solvents at different observation wavelength.

| | solvent | λ_{obs} [nm] | τ [ns] | χ_{r}^2 |
|-----------------------|---------|--------------------------------|----------------|---------------------|
| A ^a | CX | | 4.9 | |
| DCA | CX | 450 | 11.5 | 1.01 |
| | | 540 | 11.6 | 1.02 |
| | BE | 450 | 12.0 | 0.99 |
| | | 540 | 11.9 | 0.96 |
| | TH | 450 | 11.5 | 1.08 |
| | | 540 | 11.5 | 1.05 |
| | PC | 450 | 13.3 | 1.02 |
| | | 540 | 13.3 | 0.97 |

^a from ref. 32

Table S 6: Fluorescence lifetimes of deoxygenated solutions of the **Q**-series in various solvents at different observation wavelength. Maximal count numbers were approx. 2000.

| | solvent | λ_{obs} [nm] | τ_1 [ns] | A_2/A_1 | τ_2 [ns] | χ_{r}^2 |
|-----------|---------|--------------------------------|------------------|-----------|------------------|---------------------|
| Q1 | CX | 467 | 15.8 | 1.7 | 2.3 | 1.08 |
| | | 570 | 16.7 | −0.6 | 2.2 | 1.07 |
| | BE | 467 | 17.0 | 3.3 | 2.4 | 1.02 |
| | | 570 | 17.9 | −0.5 | 2.4 | 1.04 |
| | TH | 467 | 17.1 | 5.9 | 2.1 | 0.96 |
| | | 570 | 17.8 | −0.5 | 2.2 | 1.01 |
| | PC | 467 | 17.9 | 7.4 | 2.2 | 0.98 |
| | | 570 | 18.6 | −0.5 | 2.6 | 1.08 |
| Q2 | CX | 488 | 8.7 | | | 1.03 |
| | | 520 | 8.7 | | | 1.14 |
| | | 575 | 8.6 | | | 1.07 |
| | BE | 488 | 8.9 | | | 1.06 |
| | | 575 | 8.9 | | | 0.99 |
| | TH | 500 | 9.9 | | | 1.08 |
| | | 610 | 9.6 | | | 1.03 |
| | PC | 520 | 8.8 | | | 0.92 |
| | | 575 | 8.9 | | | 1.06 |
| Q3 | CX | 488 | 4.6 | | | 0.94 |
| | | 540 | 4.5 | | | 1.17 |
| | | 590 | 4.6 | | | 1.18 |
| | BE | 500 | 5.2 | | | 1.18 |
| | | 575 | 5.1 | | | 1.17 |
| | TH | 520 | 5.8 | | | 1.05 |
| | | 690 | 5.7 | | | 1.06 |
| | PC | 540 | 0.6 | | | 1.12 |
| | | 670 | 0.7 | | | 0.96 |

7 Additional Computational Results

Table S7: Calculated ground (gr-st) and excited state properties of **DCA** and the **Q**-series. τ^{2P} is the integrated two-photon absorption coefficient for a given transition and α_M is the angle between the transition dipole moment, M_a , and the axis connecting the 2 CN-groups (from position 10 to 9, as shown in Figs. S7-9). μ_i is the permanent dipole moment of state i and β_μ its angle with the axis connecting the 2 CN-groups. Q_{xx} and Q_{yy} are the two independent diagonal components of the traceless quadrupole tensor. A_Q denotes the amplitude of the quadrupole moment and B_Q its asymmetry.

| | State | ΔE [kK] | M_a [D] | α_M [°] | τ^{2P} [GM] | μ_i [D] | β_μ [°] | Q_{xx} [DÅ] | Q_{yy} [DÅ] | A_Q [DÅ] | B_Q [DÅ] |
|-----------|--------|--------------------|--------------|-------------------|---------------------|----------------|--------------------|------------------|------------------|---------------|---------------|
| D1 | gr-st | | | | | 2.14 | 62 | 35.1 | −28.5 | 45.6 | 63.6 |
| | 2(1)A' | 24.59 | 3.67 | 149 | 0.5 | 6.33 | 98 | 44.5 | −36.0 | 57.8 | 80.5 |
| | 3(1)A' | 30.37 | 2.23 | 50 | 0.1 | 1.97 | 71 | 39.2 | −31.8 | 51.0 | 71.0 |
| | 4(1)A' | 35.57 | 2.52 | 117 | 3.4 | 1.23 | 78 | 46.6 | −37.5 | 60.5 | 84.1 |
| | 5(1)A' | 41.13 | 8.60 | 79 | 1.6 | 5.66 | 88 | 40.7 | −32.7 | 52.8 | 73.4 |
| | 6(1)A' | 42.36 | 0.18 | 68 | | 2.43 | 80 | 43.0 | −33.9 | 55.5 | 76.9 |
| D2 | gr-st | | | | | 2.45 | 148 | 30.3 | −17.6 | 37.3 | 47.9 |
| | 2(1)A' | 24.87 | 3.96 | 67 | 4.4 | 11.98 | 119 | 42.1 | −27.0 | 52.2 | 69.1 |
| | 3(1)A' | 28.92 | 3.41 | 139 | 2.3 | 3.37 | 131 | 35.7 | −20.6 | 43.9 | 56.4 |
| | 4(1)A' | 33.17 | 5.92 | 123 | 14.7 | 8.68 | 125 | 51.8 | −30.8 | 63.9 | 82.7 |
| | 5(1)A' | 37.20 | 6.33 | 110 | 2.0 | 5.50 | 130 | 40.4 | −24.8 | 49.9 | 65.2 |
| | 6(1)A' | 37.95 | 2.47 | 84 | 0.1 | 7.28 | 126 | 41.2 | −24.7 | 50.8 | 65.9 |
| | 7(1)A' | 39.40 | 4.46 | 104 | | 8.88 | 122 | 48.1 | −28.8 | 59.3 | 76.9 |
| D3 | gr-st | | | | | 2.70 | 148 | 38.4 | −20.3 | 47.0 | 58.7 |
| | 2(1)A' | 25.29 | 4.71 | 75 | 8.4 | 13.58 | 119 | 48.6 | −29.2 | 59.9 | 77.7 |
| | 3(1)A' | 28.70 | 3.97 | 136 | 5.6 | 4.25 | 128 | 46.4 | −24.5 | 56.9 | 70.9 |
| | 4(1)A' | 32.49 | 6.95 | 121 | 25.4 | 11.96 | 123 | 65.1 | −36.1 | 79.9 | 101.2 |
| | 5(1)A' | 36.83 | 6.64 | 69 | 2.7 | 6.07 | 133 | 50.9 | −29.1 | 62.5 | 80.0 |
| | 6(1)A' | 38.49 | 5.05 | 72 | | 12.27 | 121 | 61.8 | −34.9 | 75.9 | 96.7 |

Table S 8: Calculated ground (gr-st) and excited state properties of **DCA** and the **Q**-series. τ^{2P} is the integrated two-photon absorption coefficient for a given transition and α_M is the angle between the transition dipole moment, M_a and the axis connecting the 2 CN-groups. Q_{xx} and Q_{yy} are the two independent diagonal components of the traceless quadrupole tensor. A_Q denotes the amplitude of the quadrupole moment and B_Q its asymmetry.

| | State | ΔE [kK] | M_a [D] | α_M [°] | τ^{2P} [GM] | Q_{xx} [DÅ] | Q_{yy} [DÅ] | A_Q [DÅ] | B_Q [DÅ] |
|------------|---------------------|--------------------|--------------|-------------------|---------------------|------------------|------------------|---------------|---------------|
| DCA | gr-st | | | | | 27.7 | −24.3 | 37.0 | 52.0 |
| | 1(1)B _{2u} | 27.58 | 3.77 | 0 | | 33.1 | −28.5 | 44.0 | 61.7 |
| | 1(1)B _{3u} | 31.08 | 1.42 | 90 | | 30.2 | −26.8 | 40.5 | 57.0 |
| | 1(1)B _{1g} | 37.47 | 0.00 | | 1.19 | 37.5 | −32.9 | 50.1 | 70.5 |
| | 2(1)B _{3u} | 43.41 | 9.43 | 90 | | 31.0 | −26.9 | 41.3 | 57.9 |
| | 2(1)B _{2u} | 44.03 | 1.64 | 180 | | 22.6 | −19.9 | 30.3 | 42.5 |
| | 2(1)A _g | 44.96 | 0.00 | | 5.61 | 30.1 | −26.2 | 40.1 | 56.3 |
| | 2(1)B _{1g} | 47.01 | 0.00 | | 3.40 | 19.2 | −17.0 | 25.7 | 36.2 |
| | 3(1)B _{2u} | 47.40 | 2.32 | 0 | | 27.7 | −24.3 | 37.0 | 52.0 |
| | 3(1)A _g | 49.09 | 0.00 | | 9.89 | 30.7 | −26.7 | 40.8 | 57.3 |
| | 3(1)B _{3u} | 52.26 | 2.92 | 90 | | 27.1 | −24.9 | 36.9 | 52.0 |
| | 4(1)A _g | 55.38 | 0.00 | | | 29.2 | −26.1 | 39.3 | 55.3 |
| | 3(1)B _{1g} | 60.73 | 0.00 | | | 32.9 | −29.4 | 44.3 | 62.3 |
| Q1 | gr-st | | | | | 44.9 | −34.0 | 57.4 | 78.9 |
| | 1(1)B _u | 22.61 | 4.04 | 40 | | 60.9 | −45.2 | 77.4 | 106.1 |
| | 2(1)B _u | 30.78 | 1.90 | 136 | | 48.0 | −36.6 | 61.4 | 84.6 |
| | 2(1)A _g | 32.08 | 0.00 | | 9.19 | 66.9 | −49.7 | 85.1 | 116.6 |
| | 3(1)B _u | 39.18 | 9.13 | −104 | | 55.3 | −40.2 | 70.0 | 95.5 |
| | 3(1)A _g | 40.93 | 0.00 | | 28.34 | 52.0 | −38.4 | 66.0 | 90.4 |
| | 4(1)B _u | 41.83 | 5.31 | 93 | | 52.8 | −39.5 | 67.2 | 92.3 |
| | 4(1)A _g | 43.80 | 0.00 | | | 53.2 | −39.4 | 67.6 | 92.6 |
| | 5(1)B _u | 44.52 | 2.05 | 150 | | 48.1 | −35.7 | 61.1 | 83.7 |
| | 5(1)A _g | 46.38 | 0.00 | | | 51.8 | −38.1 | 65.7 | 89.8 |
| Q2 | gr-st | | | | | 51.4 | −23.7 | 63.0 | 75.1 |
| | 1(1)B _u | 23.23 | 5.72 | 96 | | 97.3 | −50.4 | 119.2 | 147.7 |
| | 2(1)B _u | 28.38 | 2.53 | 32 | | 50.6 | −23.0 | 62.1 | 73.6 |
| | 2(1)A _g | 29.25 | 0.00 | | 70.18 | 133.5 | −70.2 | 163.6 | 203.7 |
| | 3(1)B _u | 33.28 | 12.03 | 117 | | 93.7 | −46.4 | 114.7 | 140.1 |
| | 3(1)A _g | 37.41 | 0.00 | | | 73.1 | −35.9 | 89.5 | 109.0 |
| | 4(1)B _u | 38.02 | 0.69 | | | 75.5 | −37.1 | 92.5 | 112.6 |
| | 4(1)A _g | 38.40 | 0.00 | | | 86.3 | −43.1 | 105.7 | 129.4 |
| | 5(1)B _u | 39.15 | 4.98 | 101 | | 106.7 | −54.9 | 130.7 | 161.6 |
| | 5(1)A _g | 39.59 | 0.00 | | | 76.3 | −36.9 | 93.4 | 113.2 |
| | 6(1)B _u | 41.39 | 2.56 | | | 106.9 | −54.7 | 130.9 | 161.6 |
| Q3 | gr-st | | | | | 77.5 | −34.9 | 95.1 | 112.4 |
| | 1(1)B _u | 23.54 | 7.52 | 91 | | 144.3 | −72.4 | 176.8 | 216.7 |
| | 2(1)B _u | 28.12 | 2.90 | 33 | | 76.1 | −33.4 | 93.4 | 109.4 |
| | 2(1)A _g | 28.86 | 0.00 | | 148.47 | 208.6 | −106.1 | 255.5 | 314.7 |
| | 3(1)B _u | 32.18 | 12.80 | 118 | | 145.5 | −70.8 | 178.2 | 216.3 |
| | 3(1)A _g | 37.07 | 0.00 | | 13.61 | 129.4 | −63.0 | 158.5 | 192.4 |
| | 4(1)B _u | 37.84 | 6.91 | 71 | | 182.7 | −91.8 | 223.8 | 274.6 |
| | 4(1)A _g | 38.60 | 0.00 | | | 125.4 | −60.5 | 153.6 | 185.9 |
| | 5(1)B _u | 39.00 | 1.55 | 65 | | 92.9 | −43.5 | 113.8 | 136.4 |
| | 5(1)A _g | 39.01 | 0.00 | | | 95.7 | −45.0 | 117.3 | 140.6 |
| | 6(1)A _g | 41.12 | 0.00 | | | 115.5 | −55.3 | 141.5 | 170.8 |

| D1 | Dipole and Quadrupole Moments | Trans. dip. (green), 2PA (red, blue) |
|-----------|-------------------------------|--------------------------------------|
| $1^1A'$ | | |
| $2^1A'$ | | |
| $3^1A'$ | | |
| $4^1A'$ | | |
| $5^1A'$ | | |

Figure S7: Permanent (left column) and transition dipole (quadrupole) moments (right column) of the first 5 electronic states of **D1**. Note for permanent moments: The lengths of the three bars for the quadrupole moments are proportional to the square-roots of the Q_{xx} , Q_{yy} , and Q_{zz} components of the traceless quadrupole moments and the color corresponds to the sign (blue - positive, red - negative). Note for transition moments: The blue (positive) and red (negative) bars point into the direction of the principle components of the two-photon transition moment tensor and the length of the bars are proportional to the corresponding eigenvalues.

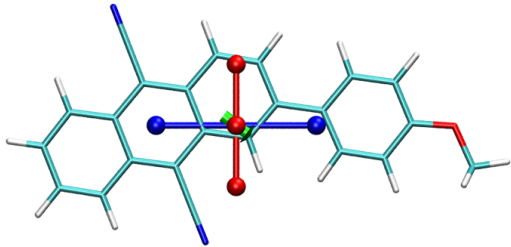
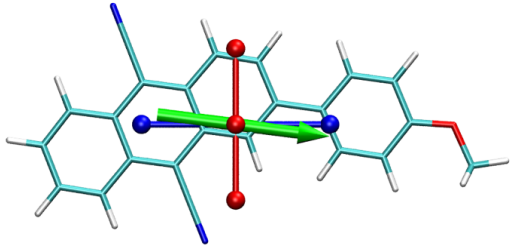
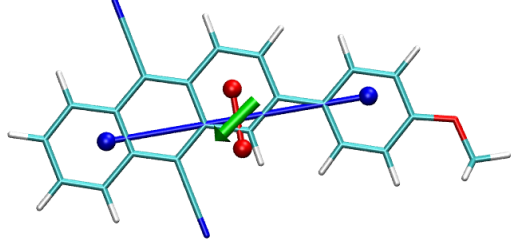
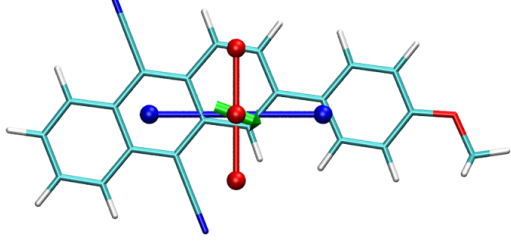
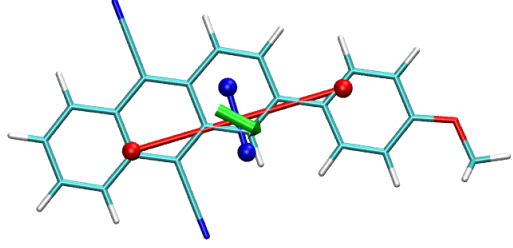
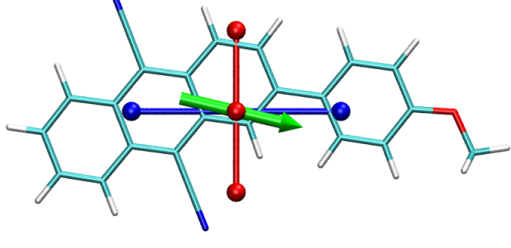
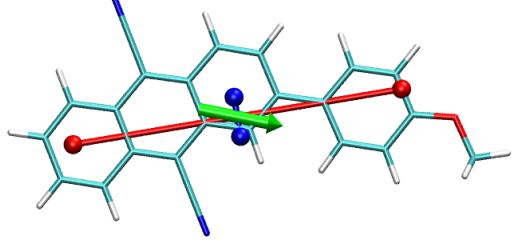
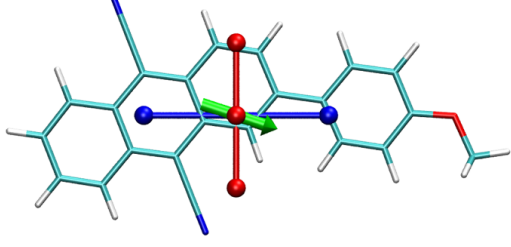
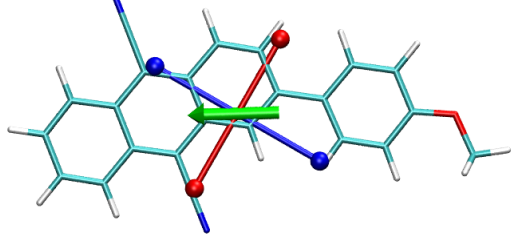
| D2 | Dipole and Quadrupole Moments | Trans. dip. (green), 2PA (red, blue) |
|---------|---|--|
| $1^1A'$ |  | |
| $2^1A'$ |  |  |
| $3^1A'$ |  |  |
| $4^1A'$ |  |  |
| $5^1A'$ |  |  |

Figure S8: Permanent (left column) and transition dipole (quadrupole) moments (right column) of the first 5 electronic states of **D2**.

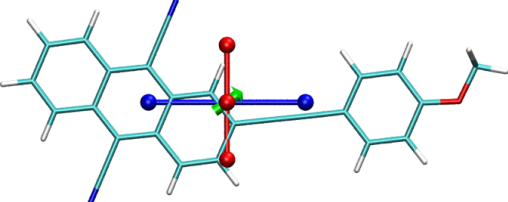
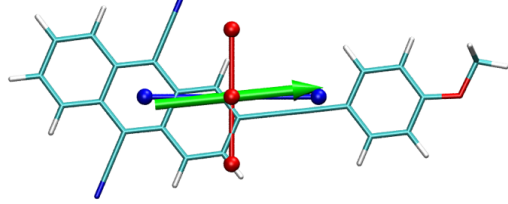
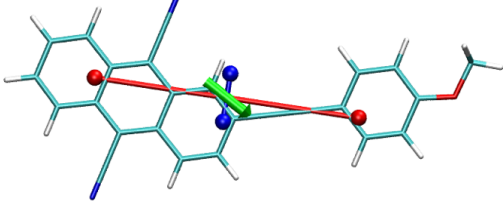
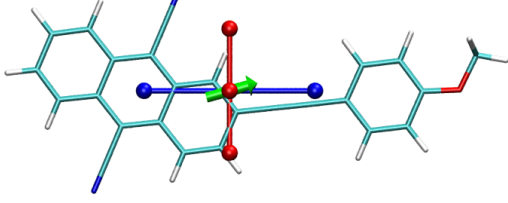
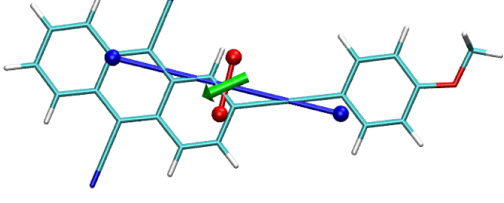
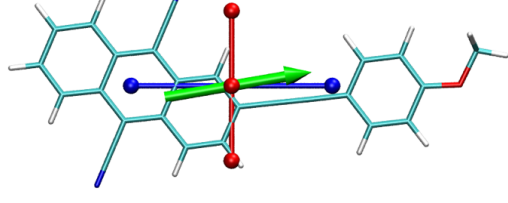
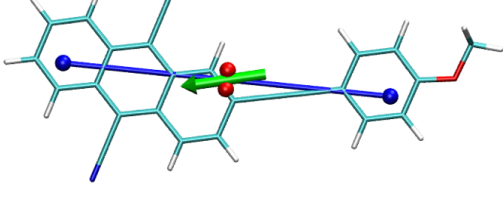
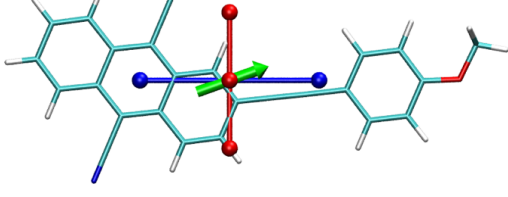
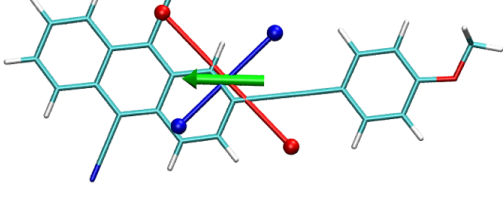
| D3 | Dipole and Quadrupole Moments | Trans. dip. (green), 2PA (red, blue) |
|-----------|---|--|
| $1^1A'$ |  | |
| $2^1A'$ |  |  |
| $3^1A'$ |  |  |
| $4^1A'$ |  |  |
| $5^1A'$ |  |  |

Figure S9: Permanent (left column) and transition dipole (quadrupole) moments (right column) of the first 5 electronic states of **D3**.

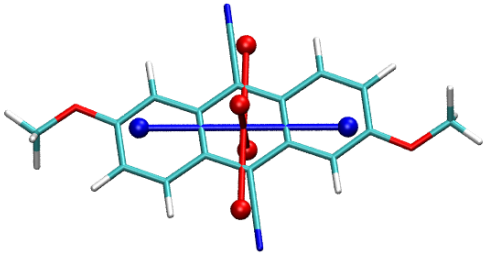
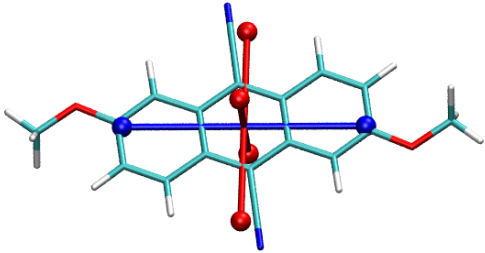
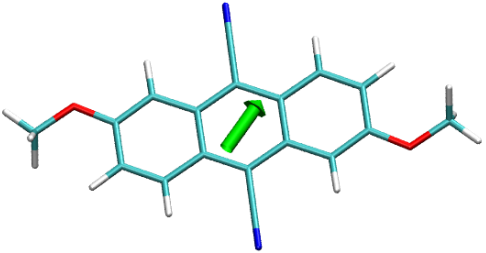
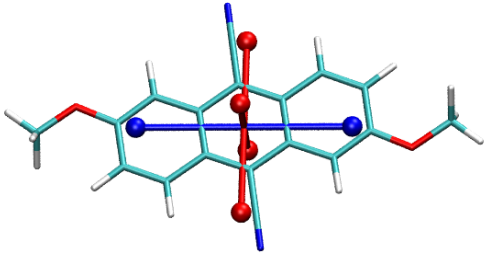
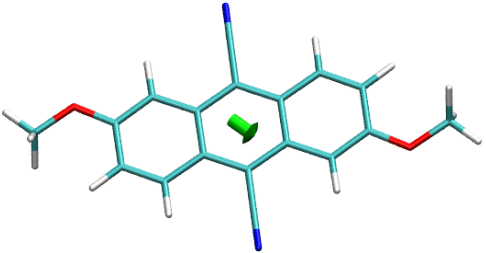
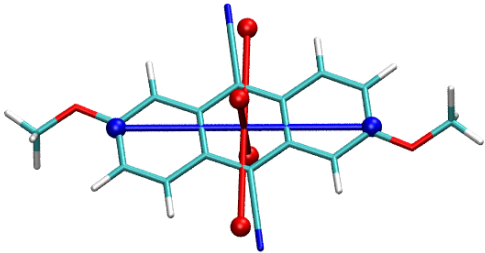
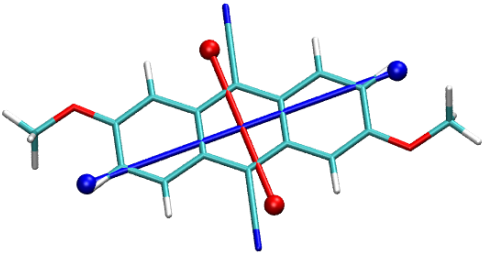
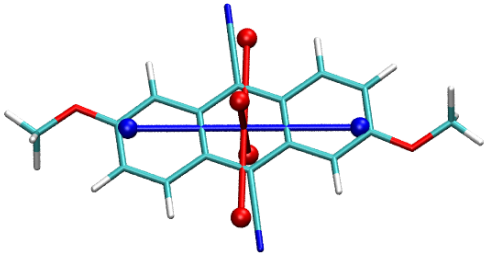
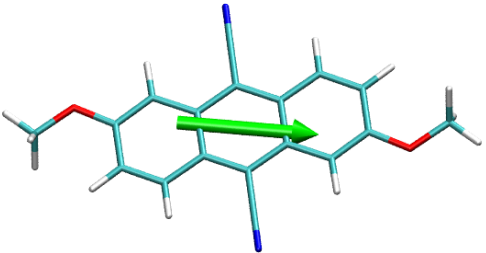
| Q1 | Quadrupole Moments | Trans. dip. (green), 2PA (red, blue) |
|----------------|---|--|
| 1^1Ag |  | |
| 1^1Bu |  |  |
| 2^1Bu |  |  |
| 2^1Ag |  |  |
| 3^1Bu |  |  |

Figure S 10: Permanent (left column) and transition dipole (quadrupole) moments (right column) of the first 5 electronic states of **Q1**.

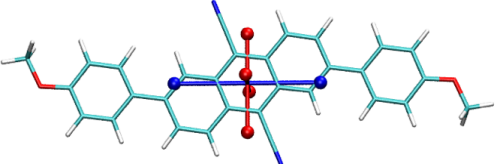
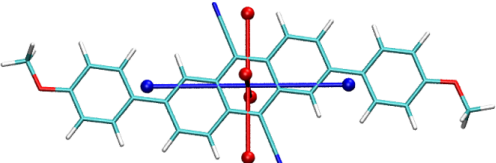
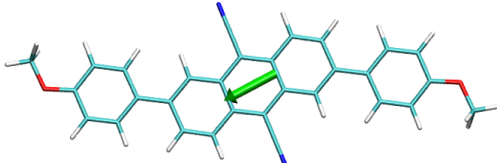
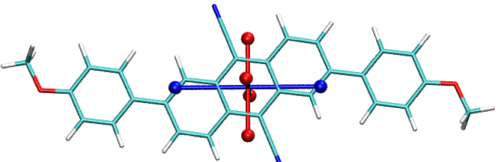
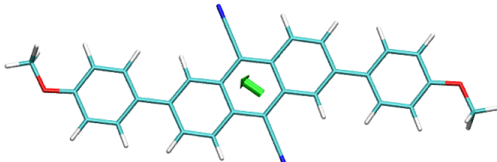
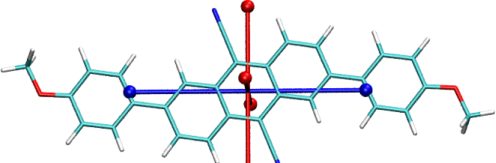
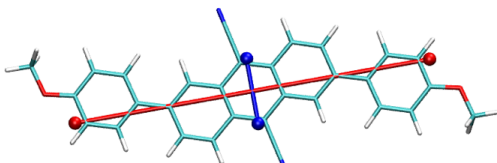
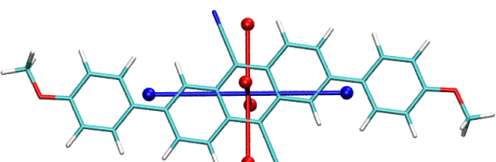
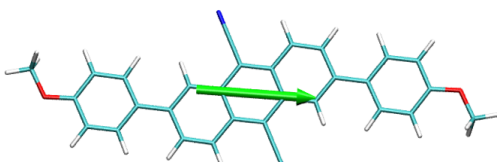
| Q2 | Quadrupole Moments | Trans. dip. (green), 2PA (red, blue) |
|----------------|---|--|
| 1^1Ag |  | |
| 1^1Bu |  |  |
| 2^1Bu |  |  |
| 2^1Ag |  |  |
| 3^1Bu |  |  |

Figure S 11: Permanent (left column) and transition dipole (quadrupole) moments (right column) of the first 5 electronic states of **Q2**.

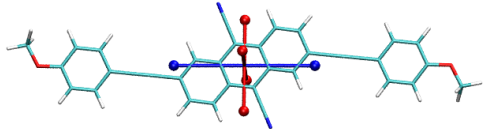
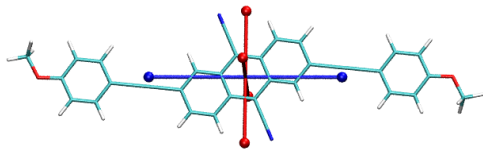
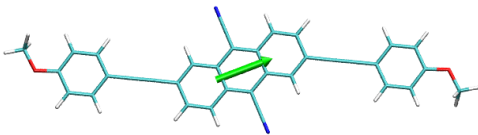
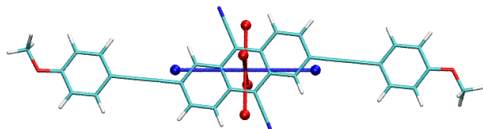
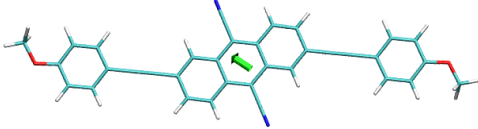
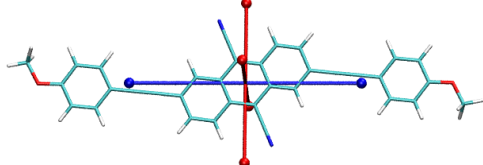
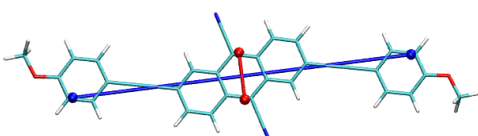
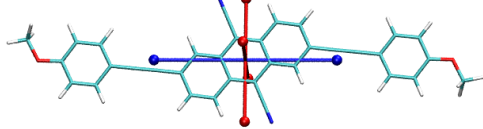
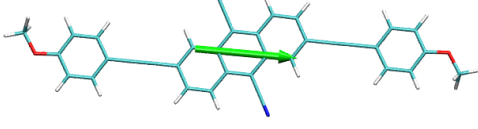
| Q3 | Quadrupole Moments | Trans. dip. (green), 2PA (red, blue) |
|----------------|---|--|
| 1^1Ag |  | |
| 1^1Bu |  |  |
| 2^1Bu |  |  |
| 2^1Ag |  |  |
| 3^1Bu |  |  |

Figure S 12: Permanent (left column) and transition dipole (quadrupole) moments (right column) of the first 5 electronic states of **Q3**.

8 NMR Spectra

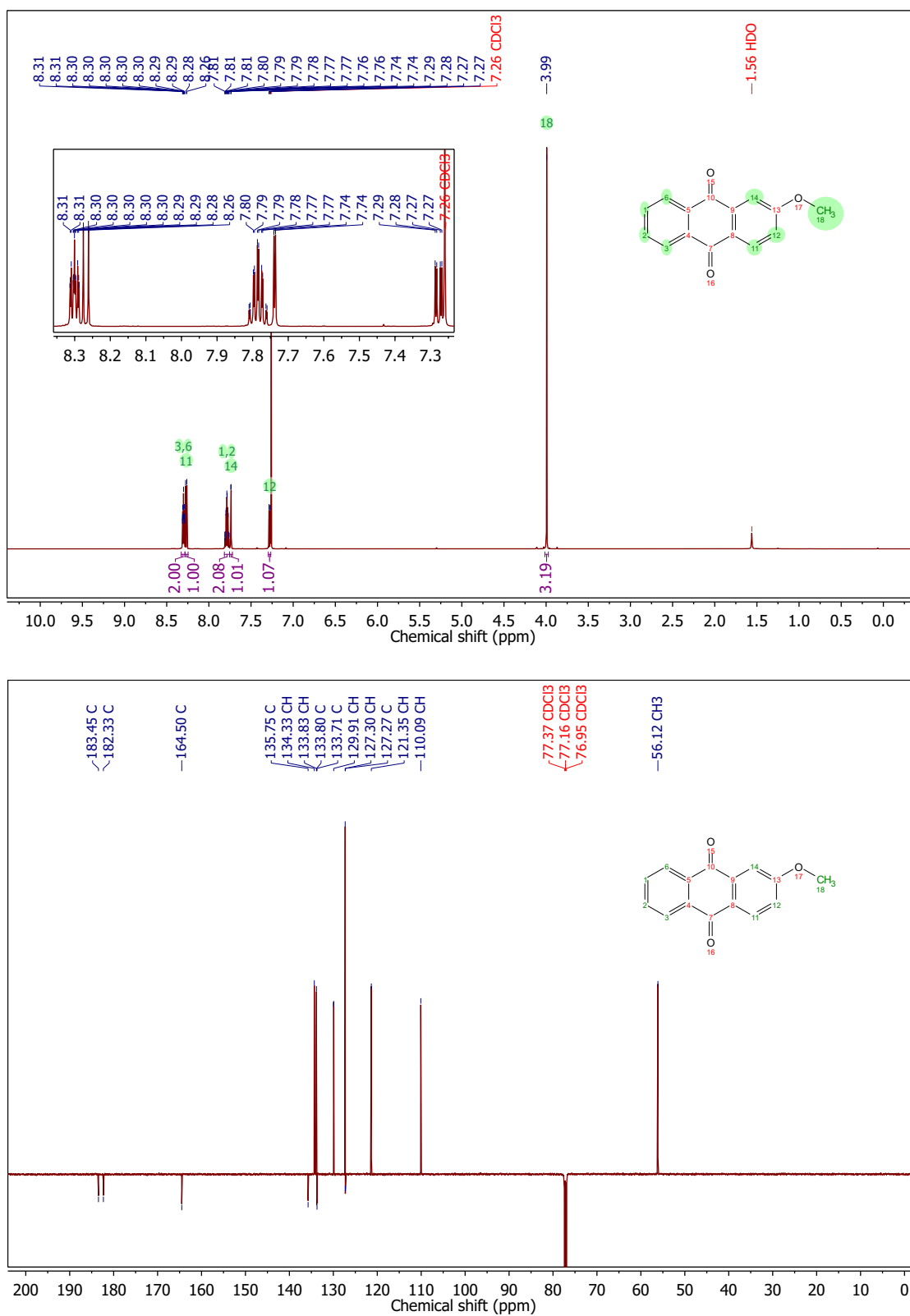


Figure S 13: ^1H and ^{13}C -NMR spectra of **2a**.

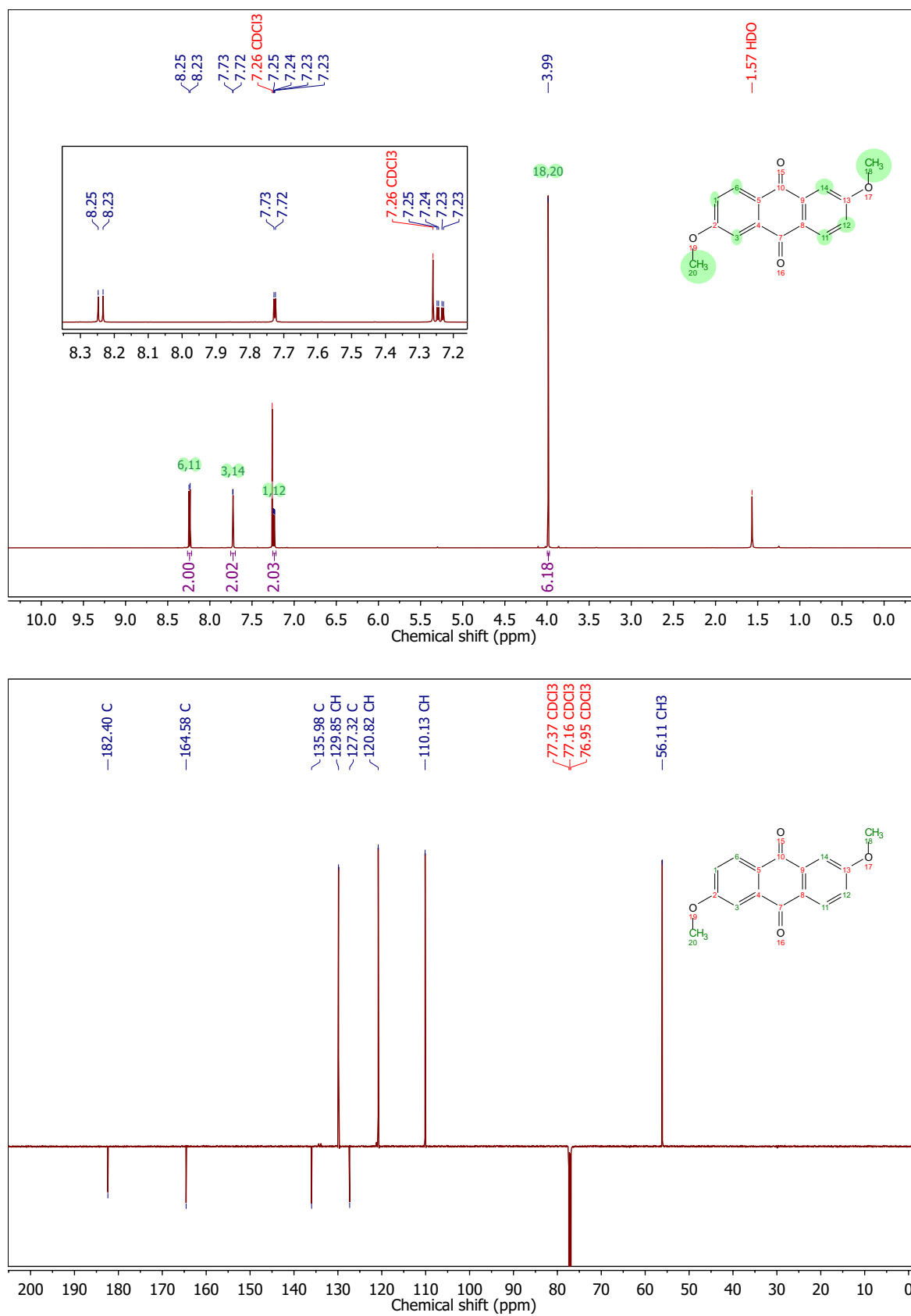


Figure S 14: ¹H and ¹³C-NMR spectra of **2b**.

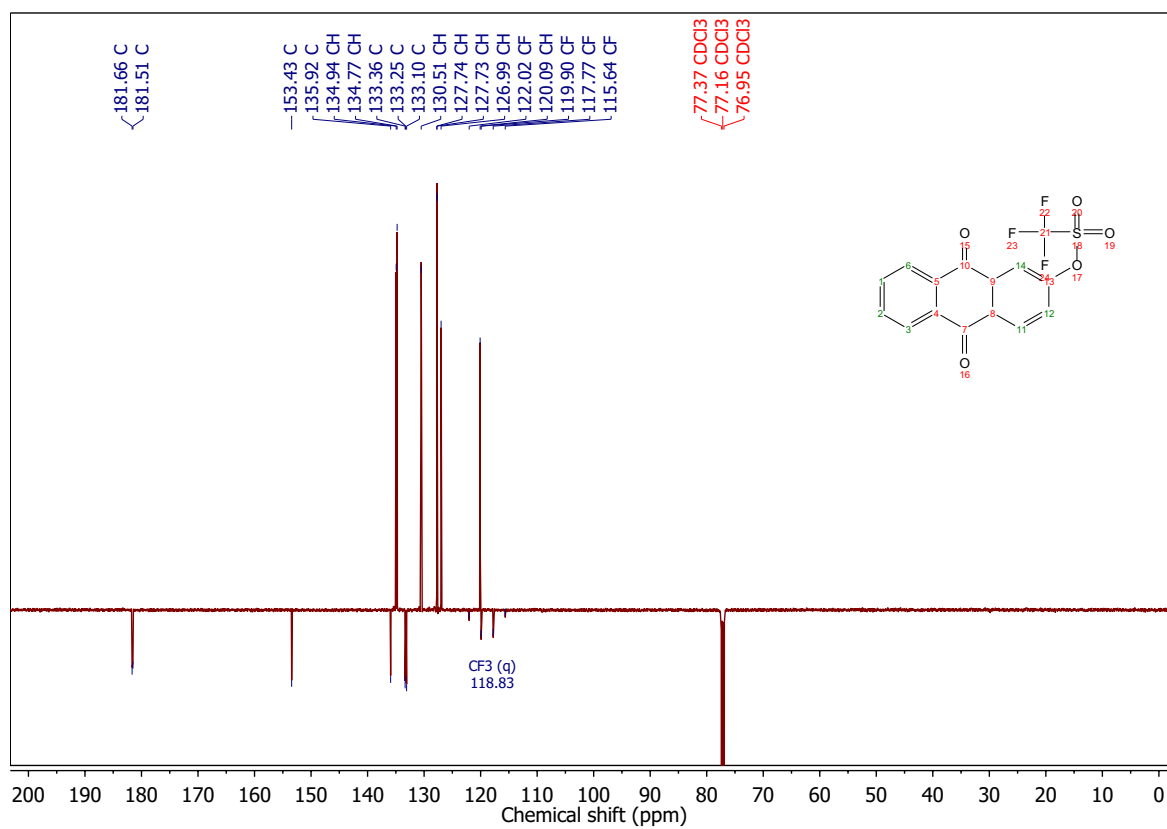
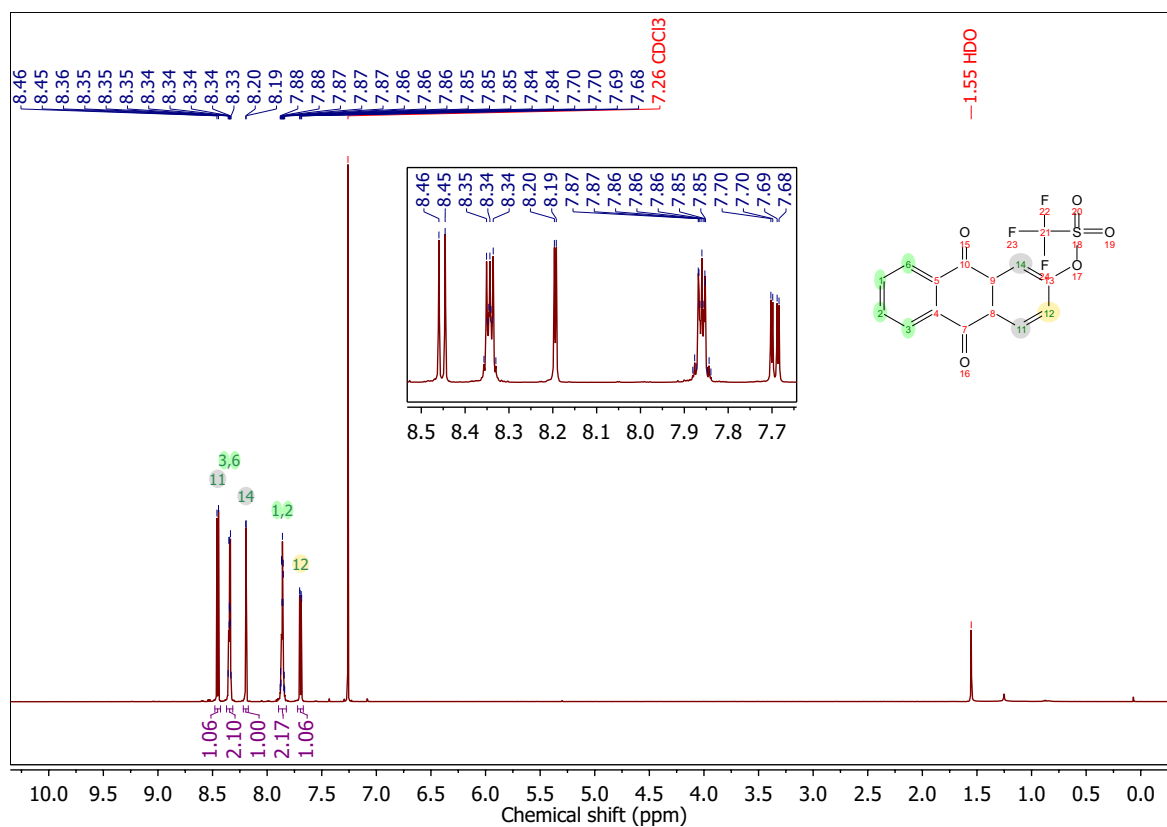


Figure S 15: ¹H and ¹³C-NMR spectra of **3a**.

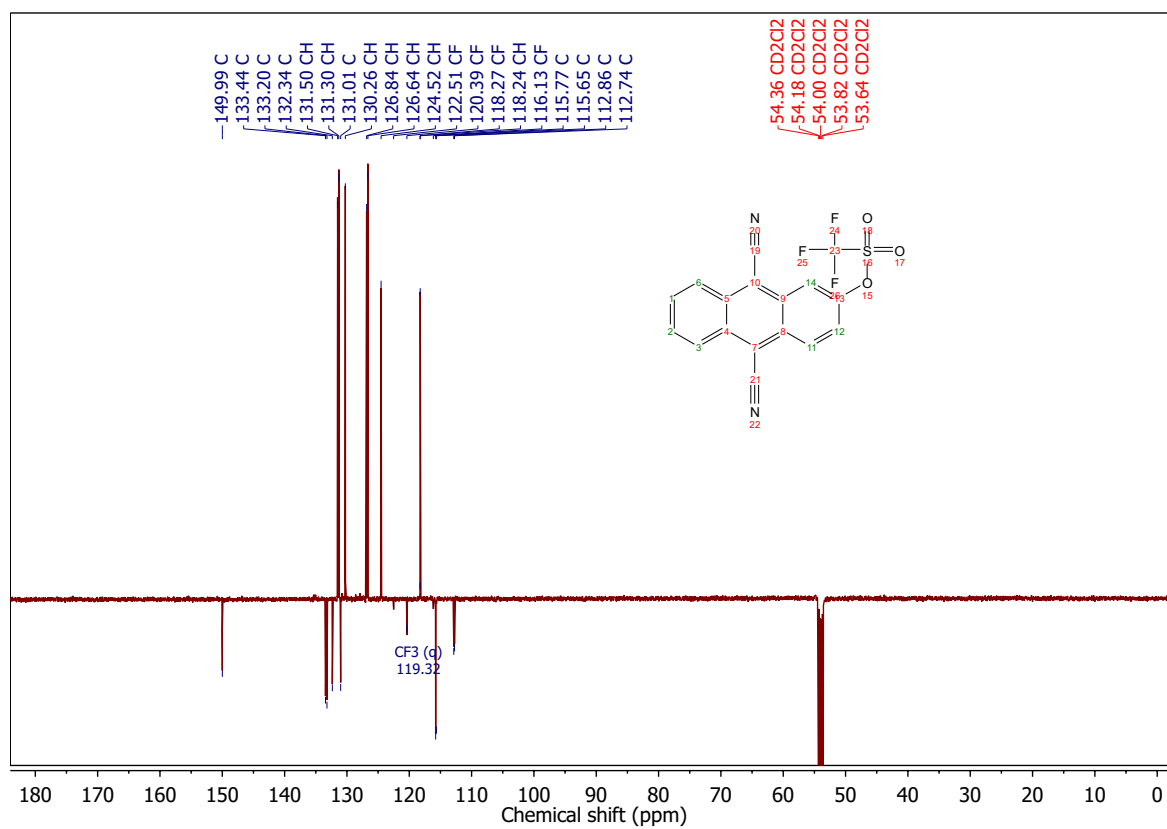
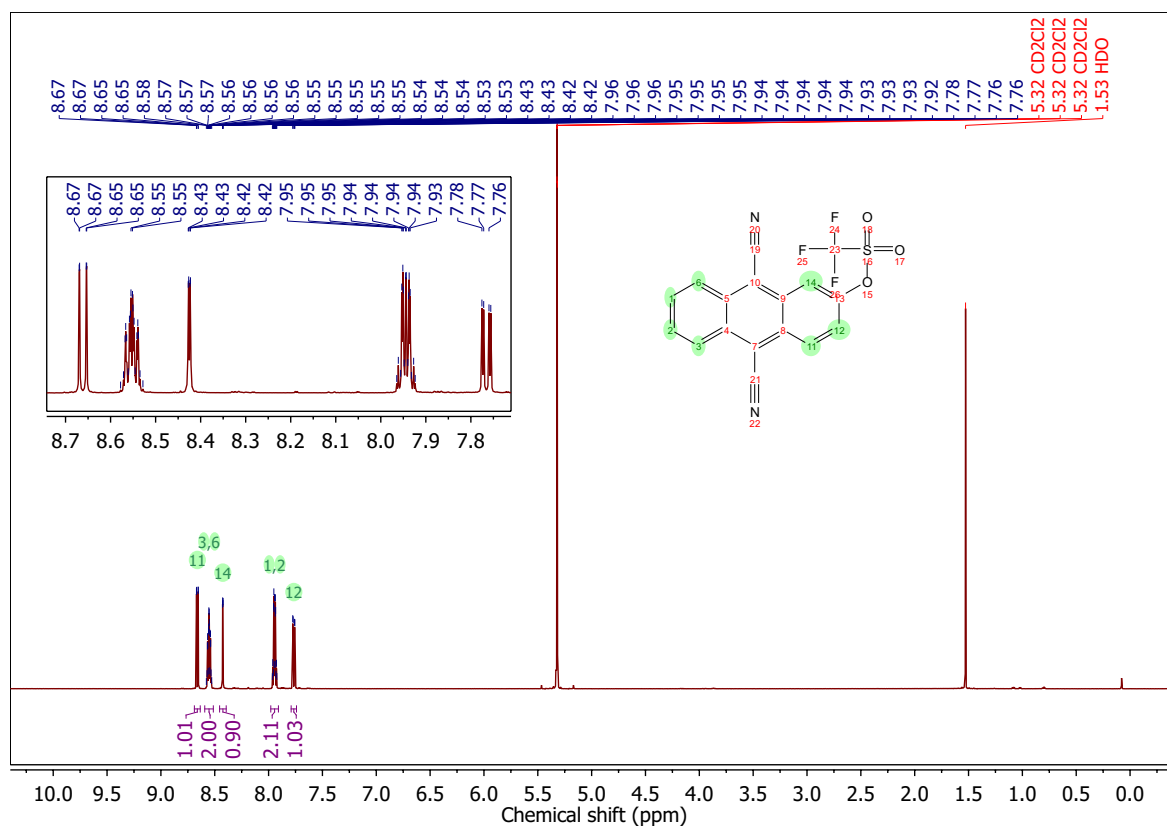


Figure S 16: ¹H and ¹³C-NMR spectra of **4a**.

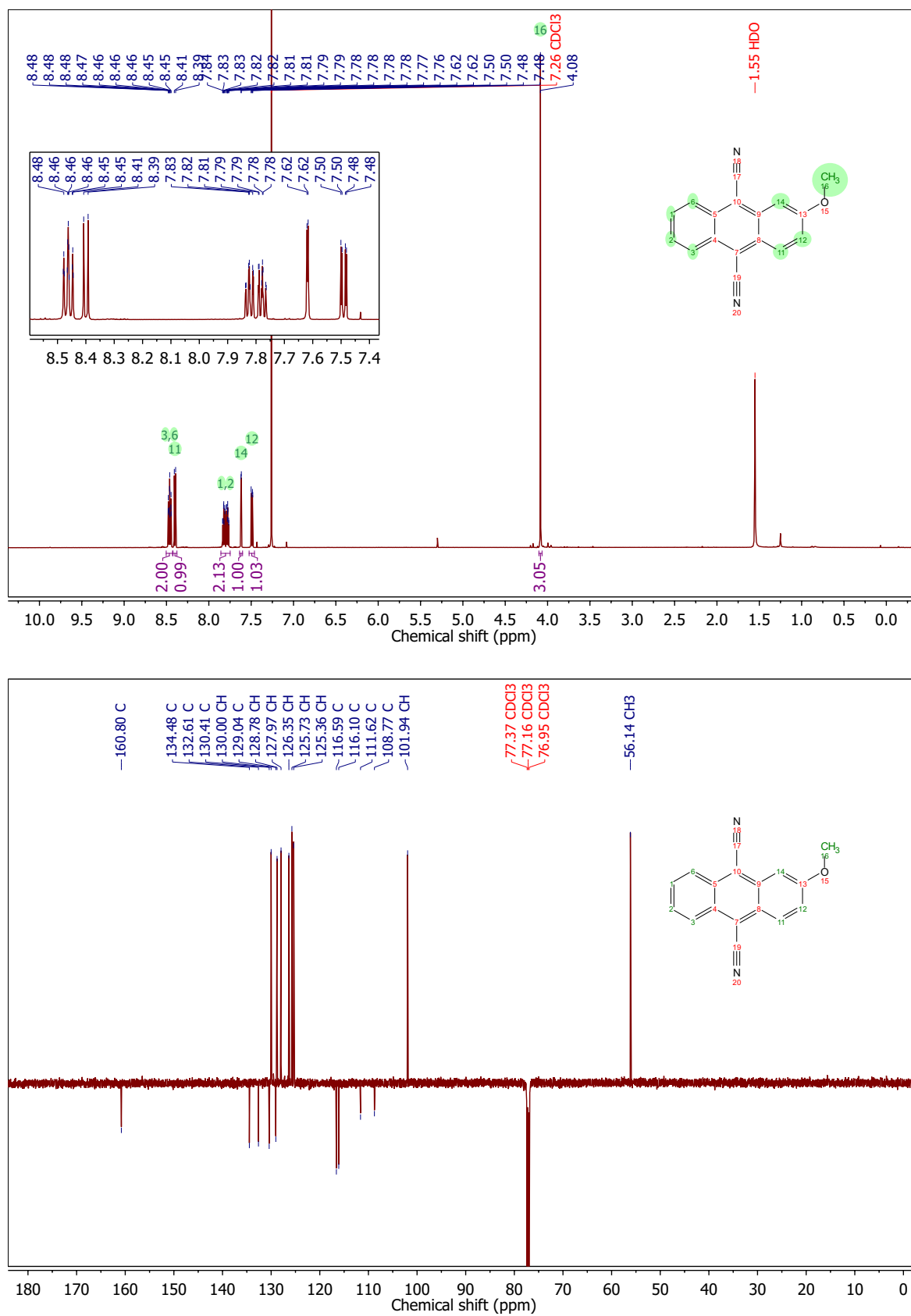


Figure S 17: ¹H and ¹³C-NMR spectra of D1.

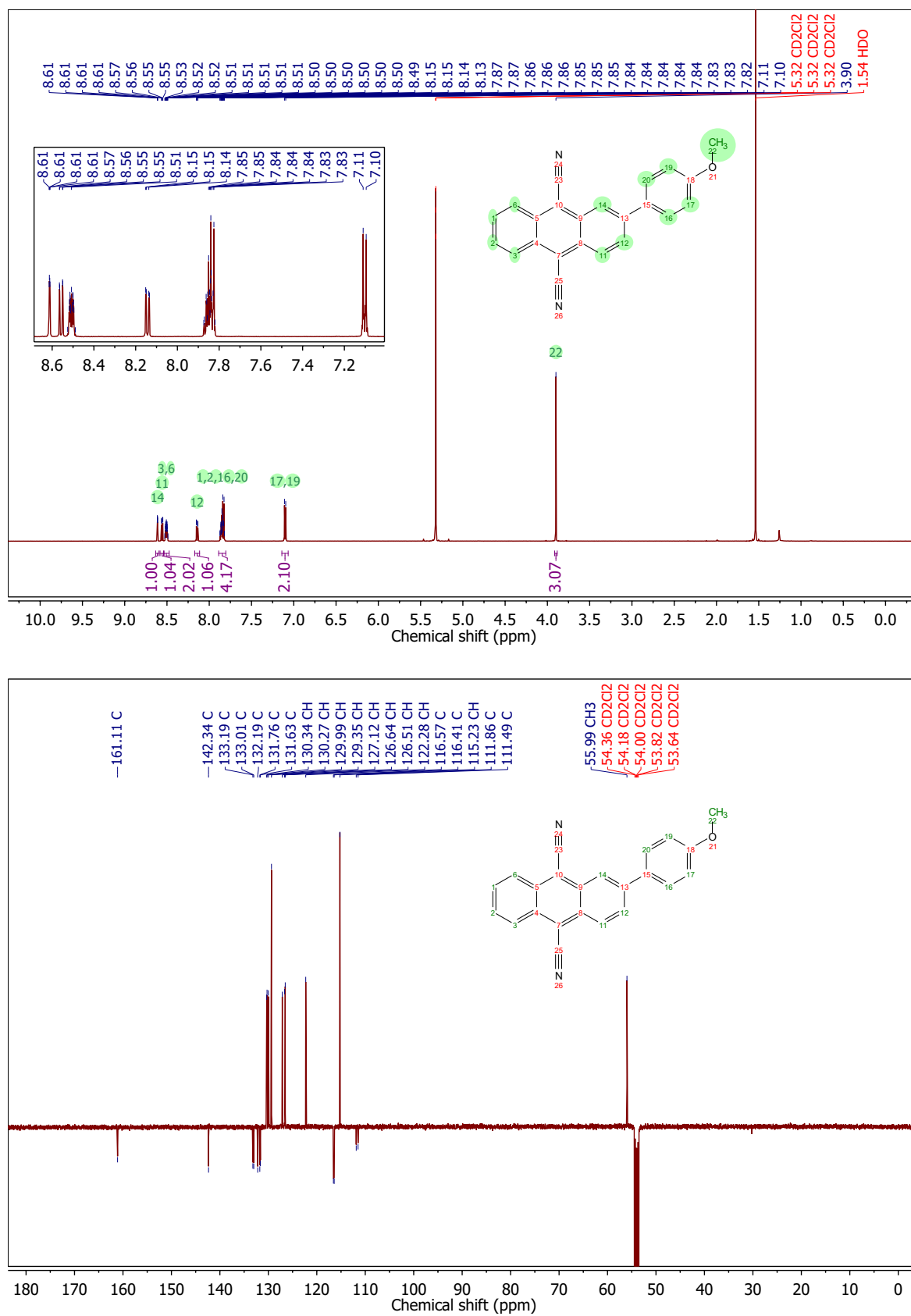


Figure S 18: ¹H and ¹³C-NMR spectra of D2.

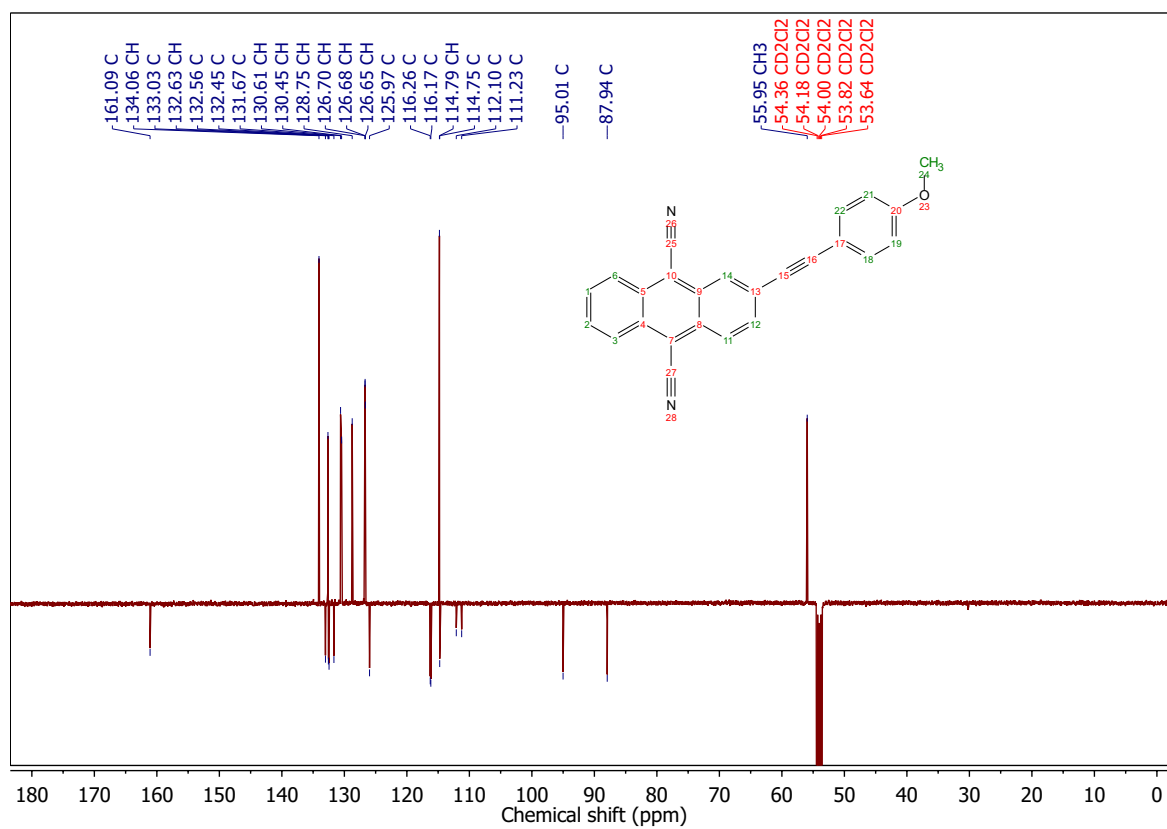
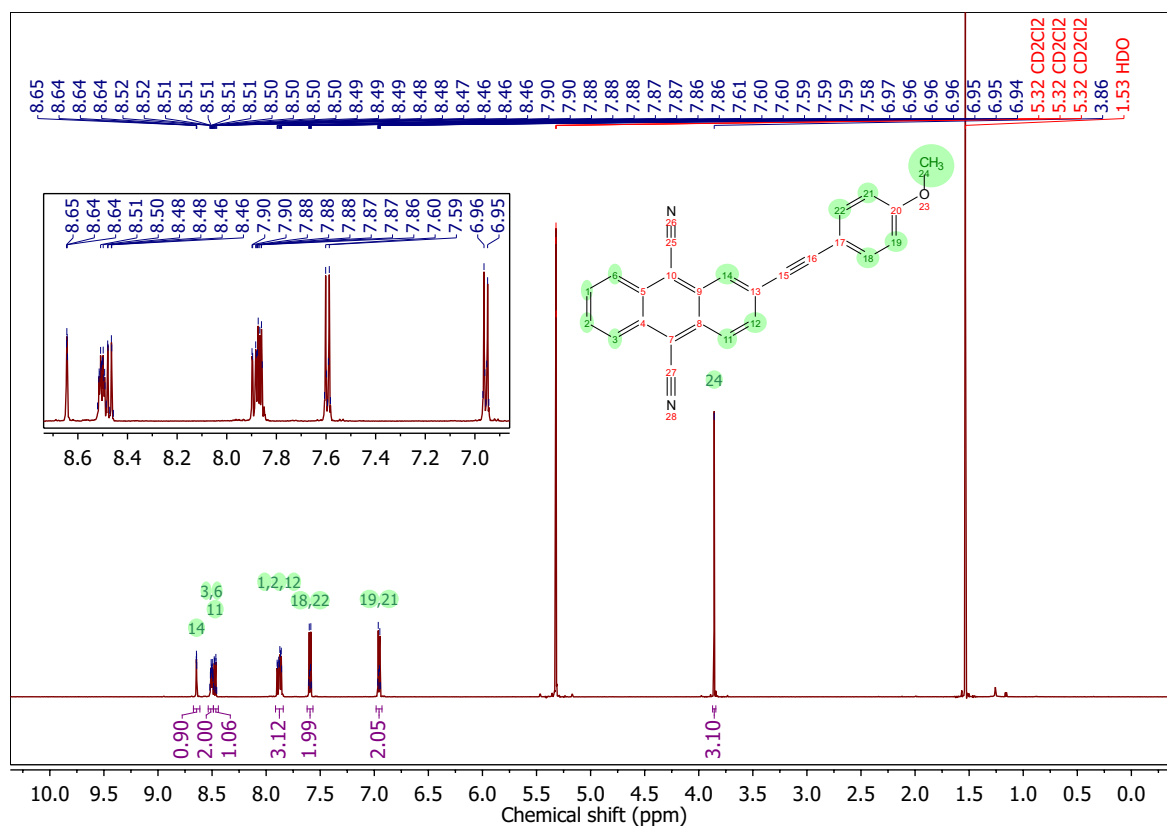


Figure S 19: ^1H and ^{13}C -NMR spectra of **D3**.

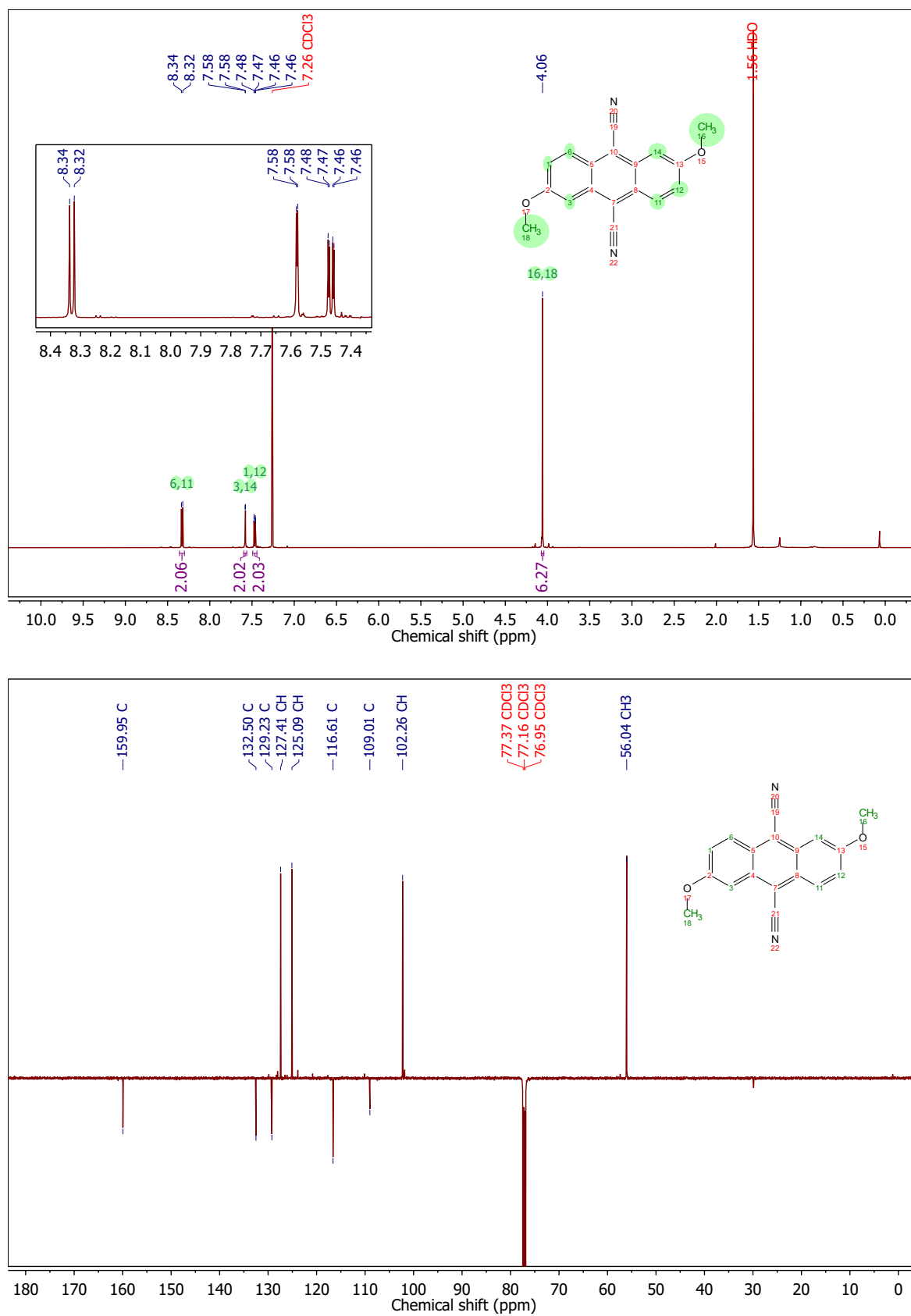


Figure S 20: ¹H and ¹³C-NMR spectra of Q1.

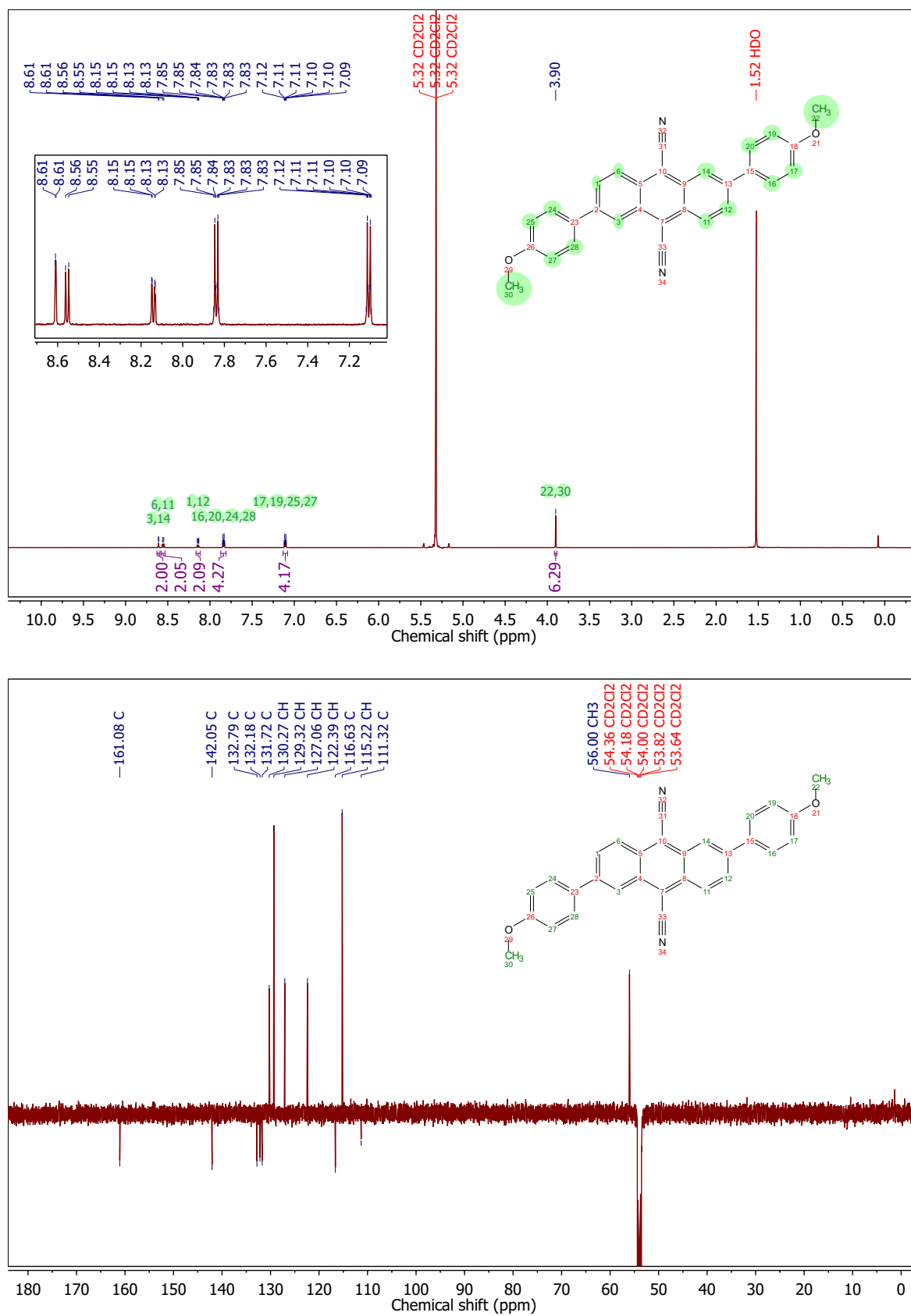


Figure S 21: ¹H and ¹³C-NMR spectra of Q2.

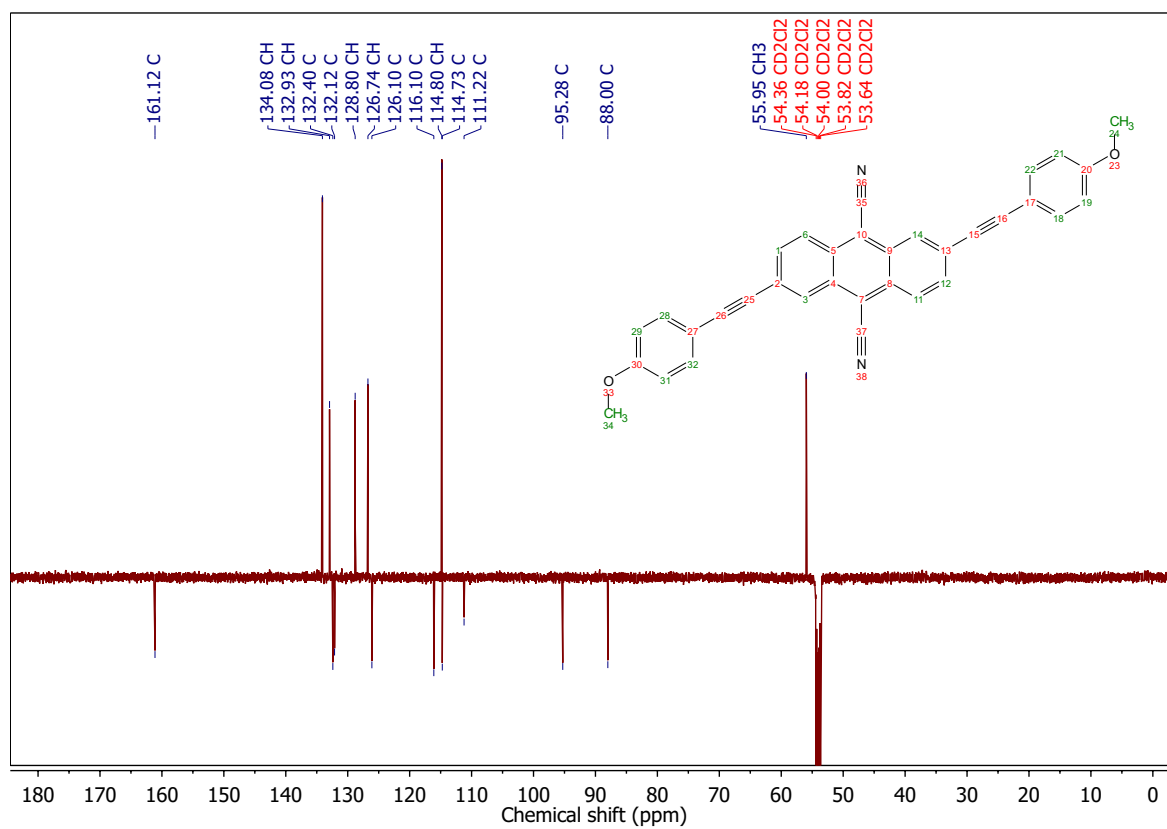
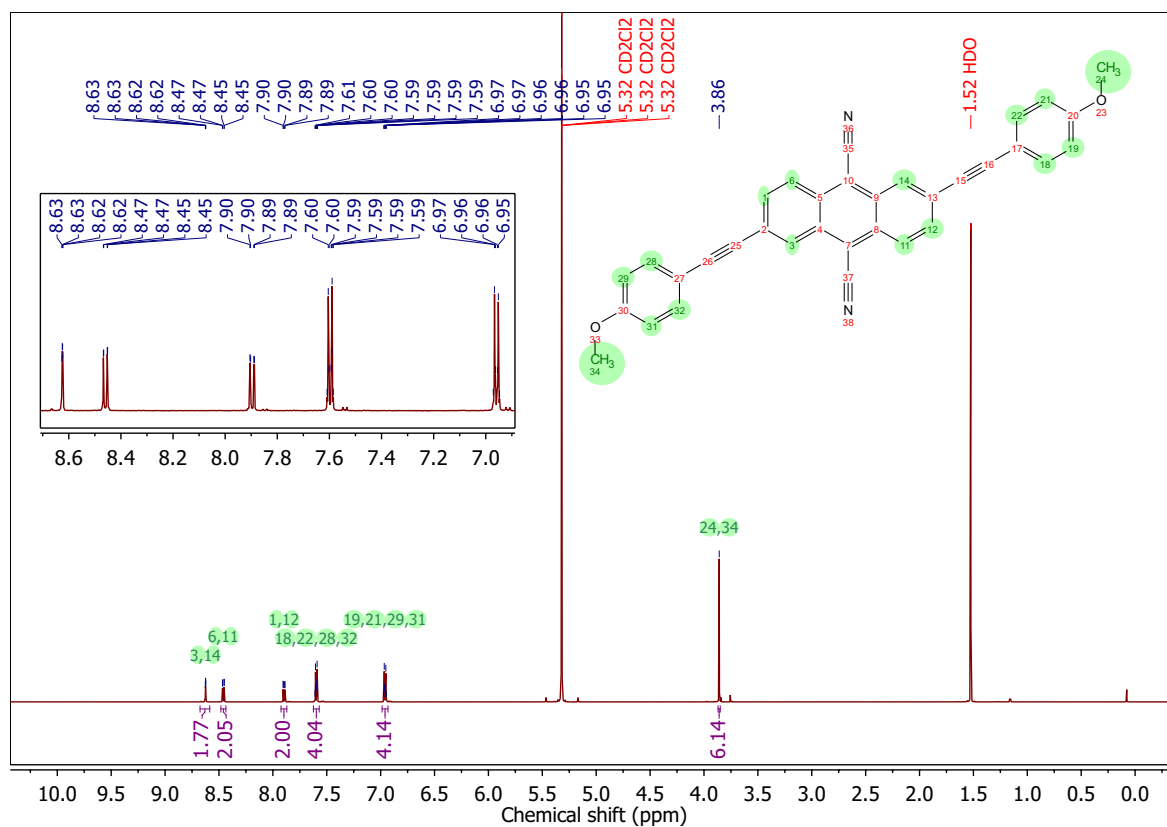


Figure S 22: ¹H and ¹³C-NMR spectra of Q3.

References

- [1] V. V. Pavlishchuk and A. W. Addison, *Inorg. Chim. Acta*, 2000, **298**, 97–102.
- [2] J. A. Gardecki and M. Maroncelli, *Appl. Spectr.*, 1998, **52**, 1179–1189.
- [3] D. Magde, R. Wong and P. G. Seybold, *Photochem. Photobiol.*, 2002, **75**, 327–334.
- [4] M. Kubista, R. Sjöback, S. Eriksson and B. Albinsson, *The Analyst*, 1994, **119**, 417–419.
- [5] S. Arzhantsev, K. A. Zachariasse and M. Maroncelli, *J. Phys. Chem. A*, 2006, **110**, 3454–3470.
- [6] J. Lewis and M. Maroncelli, *Chem. Phys. Lett.*, 1998, **282**, 197–203.
- [7] D. Topygin, *J. Flu.*, 2003, **13**, 201–219.
- [8] A. Rosspeintner, G. Angulo and E. Vauthey, *J. Am. Chem. Soc.*, 2014, **136**, 2026–2032.
- [9] N. S. Makarov, M. Drobizhev and A. Rebane, *Opt. Express*, 2008, **16**, 4029–4047.
- [10] Z. Li, A. Rosspeintner, P. Hu, G. Zhu, Y. Hu, X. Xiong, R. Peng, M. Wang, X. Liu and R. Liu, *Polym. Chem.*, 2017, **8**, 6644–6653.
- [11] Y. Lu and A. Penzkofer, *Chem. Phys.*, 1986, **107**, 175–184.
- [12] S. de Reguardati, J. Pahapill, A. Mikhailov, Y. Stepanenko and A. Rebane, *Opt. Express*, 2016, **24**, 9053.
- [13] C. Adamo and V. Barone, *J. Chem. Phys.*, 1999, **110**, 6158–6170.
- [14] A. Schafer, C. Huber and R. Ahlrichs, *J. Chem. Phys.*, 1994, **100**, 5829–5835.
- [15] A. Dreuw and M. Wormit, *Wiley Interdiscip. Rev. Comput. Mol. Sci.*, 2015, **5**, 82–95.
- [16] F. Plasser and H. Lischka, *J. Chem. Theory Comput.*, 2012, **8**, 2777–2789.
- [17] F. Plasser, M. Wormit and A. Dreuw, *J. Chem. Phys.*, 2014, **141**, 0–13.
- [18] S. Knippenberg, D. R. Rehn, M. Wormit, J. H. Starcke, I. L. Rusakova, A. B. Trofimov and A. Dreuw, *J. Chem. Phys.*, 2012, **136**, 064107.
- [19] M. Wormit, D. R. Rehn, P. H. Harbach, J. Wenzel, C. M. Krauter, E. Epifanovsky and A. Dreuw, *Mol. Phys.*, 2014, **112**, 774–784.
- [20] Y. Shao, Z. Gan, E. Epifanovsky, A. T. Gilbert, M. Wormit, J. Kussmann, A. W. Lange, A. Behn, J. Deng, X. Feng, D. Ghosh, M. Goldey, P. R. Horn, L. D. Jacobson, I. Kaliman, R. Z. Khaliullin, T. Kus, A. Landau, J. Liu, E. I. Proynov, Y. M. Rhee, R. M. Richard, M. A. Rohrdanz, R. P. Steele, E. J. Sundstrom, H. L. Woodcock, P. M. Zimmerman, D. Zuev, B. Albrecht, E. Alguire, B. Austin, G. J. Beran, Y. A. Bernard, E. Berquist, K. Brandhorst, K. B. Bravaya, S. T. Brown, D. Casanova, C. M. Chang, Y. Chen, S. H. Chien, K. D. Closser, D. L. Crittenden, M. Diedenhofen, R. A. Distasio, H. Do, A. D. Dutoi, R. G. Edgar, S. Fatehi, L. Fusti-Molnar, A. Ghysels, A. Golubeva-Zadorozhnaya, J. Gomes, M. W. Hanson-Heine, P. H. Harbach, A. W. Hauser, E. G. Hohenstein, Z. C. Holden, T. C. Jagau, H. Ji, B. Kaduk, K. Khistyayev, J. Kim, J. Kim, R. A. King, P. Klunzinger, D. Kosenkov, T. Kowalczyk, C. M. Krauter, K. U. Lao, A. D. Laurent, K. V. Lawler, S. V. Levchenko, C. Y. Lin, F. Liu, E. Livshits, R. C. Lochan, A. Luenser, P. Manohar, S. F. Manzer, S. P. Mao, N. Mardirossian, A. V. Marenich, S. A. Maurer, N. J. Mayhall, E. Neuscamman, C. M. Oana,

- R. Olivares-Amaya, D. P. Oneill, J. A. Parkhill, T. M. Perrine, R. Peverati, A. Prociuk, D. R. Rehn, E. Rosta, N. J. Russ, S. M. Sharada, S. Sharma, D. W. Small, A. Sodt, T. Stein, D. Stück, Y. C. Su, A. J. Thom, T. Tsuchimochi, V. Vanovschi, L. Vogt, O. Vydrov, T. Wang, M. A. Watson, J. Wenzel, A. White, C. F. Williams, J. Yang, S. Yeganeh, S. R. Yost, Z. Q. You, I. Y. Zhang, X. Zhang, Y. Zhao, B. R. Brooks, G. K. Chan, D. M. Chipman, C. J. Cramer, W. A. Goddard, M. S. Gordon, W. J. Hehre, A. Klamt, H. F. Schaefer, M. W. Schmidt, C. D. Sherrill, D. G. Truhlar, A. Warshel, X. Xu, A. Aspuru-Guzik, R. Baer, A. T. Bell, N. A. Besley, J. D. Chai, A. Dreuw, B. D. Dunietz, T. R. Furlani, S. R. Gwaltney, C. P. Hsu, Y. Jung, J. Kong, D. S. Lambrecht, W. Liang, C. Ochsenfeld, V. A. Rassolov, L. V. Slipchenko, J. E. Subotnik, T. Van Voorhis, J. M. Herbert, A. I. Krylov, P. M. Gill and M. Head-Gordon, *Mol. Phys.*, 2015, **113**, 184–215.
- [21] M. T. P. Beerepoot, D. H. Friese, N. H. List, J. Kongsted and K. Ruud, *Phys. Chem. Chem. Phys.*, 2015, **17**, 19306–19314.
- [22] M. de Wergifosse, C. G. Elles and A. I. Krylov, *J. Chem. Phys.*, 2017, **146**, 174102.
- [23] R. Fortrie and H. Chermette, *J. Chem. Phys.*, 2006, **124**, 204104.
- [24] K. Saha, K. W. Lam, F. Abas, A. S. Hamzah, J. Stanslas, L. S. Hui and N. H. Lajis, *Med. Chem. Res.*, 2013, **22**, 2093–2104.
- [25] T. S. Navale and R. Rathore, *Synthesis*, 2012, **44**, 805–809.
- [26] Y. Hou, L. A. Huck and P. Wan, *Photochem. Photobiol. Sci.*, 2009, **8**, 1408–1415.
- [27] J. E. Gautrot, P. Hodge, D. Cupertino and M. Helliwell, *New J. Chem.*, 2007, **31**, 1585–1593.
- [28] F. Glöckhofer, P. Kautny, P. Fritz, B. Stöger and J. Fröhlich, *ChemPhotoChem*, 2016, **1**, 51–55.
- [29] R. O. Loutfy and R. O. Loutfy, *Can. J. Chem.*, 1976, **54**, 1454–1463.
- [30] D. York, N. M. Evensen, M. L. Martínez and J. De Basabe Delgado, *Am. J. Phys.*, 2004, **72**, 367–375.
- [31] N. Ghoneim and P. Suppan, *Spectrochim. Acta, Part A*, 1995, **51**, 1043–1050.
- [32] I. B. Berlman, *Handbook of Fluorescence Spectra of Aromatic Molecules*, Academic Press Inc, New York, 2nd edn, 1971.